Maternal diet and gut microbiome composition modulate early life immune development

Erica T Grant[1,2], Marie Boudaud[1], Arnaud Muller[3,4], Andrew J Macpherson[5], and Mahesh S Desai[1,6,*]

[1]Department of Infection and Immunity, Luxembourg Institute of Health, Esch-sur-Alzette, Luxembourg

[2]Faculty of Science, Technology and Medicine, University of Luxembourg, Esch-sur-Alzette, Luxembourg

[3]Bioinformatics Platform, Data Integration and Analysis, Luxembourg Institute of Health, Strassen, Luxembourg

[4]LuxGen, Translational Medicine Operation Hub, Luxembourg Institute of Health, Dudelange, Luxembourg

[5]Department of Visceral Surgery and Medicine, Bern University Hospital, University of Bern, 3010, Bern, Switzerland.

[6]Odense Research Center for Anaphylaxis, Department of Dermatology and Allergy Center, Odense University Hospital, University of Southern Denmark, Odense, Denmark

*Correspondence: mahesh.desai@lih.lu

Abstract

In early life, the intestinal mucosa and immune system undergo a critical developmental process to contain the expanding gut microbiome while promoting tolerance towards commensals, yet the influence of maternal diet and gut microbial composition on offspring immune maturation remains poorly understood. We colonized gnotobiotic mice with a defined consortium of 14 strains, fed them a standard fiber-rich chow or a fiber-free diet, and then longitudinally assessed offspring development during the weaning period. Unlike pups born to dams fed the fiber-rich diet, pups of fiber-deprived dams demonstrated delayed colonization with *Akkermansia muciniphila*, a mucin-foraging bacterium that can also utilize milk oligosaccharides. The pups of fiber-deprived dams exhibited an enrichment of colonic tissue transcripts corresponding to defense response pathways and a peak in *Il22* expression at weaning. Removal of *A. muciniphila* from the community, but maintenance on the fiber-rich diet, was associated with reduced proportions of RORγt-positive innate and adaptive immune cell subsets. Our results highlight the potent influence of maternal dietary fiber intake and discrete changes in microbial composition on the postnatal microbiome assemblage and early immune development.

Introduction

Dietary fiber plays a major role in shaping the colonic gut microbiome and host immunity, however the impact of maternal dietary fiber intake on the offspring's microbiome and immune development is largely associative for the early life period (Mirpuri, 2021). In adult mice, dietary fiber deprivation leads to microbiome-driven thinning of the mucus layer, which can increase susceptibility to a range of conditions including enteric pathogen infection (Desai *et al.*, 2016; Neumann *et al.*, 2021), graft-versus-host disease (Hayase *et al.*, 2022), and food allergy (Parrish, Boudaud, *et al.*, 2022). Although exposure to microbial metabolites in utero initiates innate immune responses and barrier development in pups (De Agüero *et al.*, 2016), the postnatal period is also critical for healthy maturation of intestinal function and adaptive immunity in a complex process that is partially driven by a response to the colonizing microbiome (Kalbermatter *et al.*, 2021; Wells *et al.*, 2022). In particular, from 2–4 weeks of age, mouse pups transition from breast milk to solid food with an accompanying shift in microbial composition and a vigorous immune response to the expanding microbiota (Al Nabhani *et al.*, 2019). Without this "weaning reaction", as observed in germ-free and broad-spectrum antibiotic-treated mice, Al Nabhani *et al* reported increased susceptibility to inflammatory pathologies (Al Nabhani *et al.*, 2019). However, it remains unclear how variations in the maternal diet or defined differences in microbial composition affect early life immune profile (Ansaldo *et al.*, 2019).

We therefore set out to investigate the influence of maternal dietary fiber intake on the offspring colonic development by feeding dams either a standard fiber-rich (FR) chow or a custom fiber-free (FF) diet (Desai *et al.*, 2016) (**Fig 1A**). To standardize the bacterial composition and facilitate interpretation of the microbial shifts, we utilized a gnotobiotic mouse model consisting of 14 bacterial strains (14-member synthetic human gut microbiota or 14SM) that form a functionally diverse community (Desai *et al.*, 2016; Steimle *et al.*, 2021). Although this community was designed to resemble an adult microbiota, one member—*Akkermansia muciniphila*—is capable of degrading milk oligosaccharides (Kostopoulos *et al.*, 2020; Luna *et al.*, 2022) and is an early colonizer of the gut

63 (Collado *et al.*, 2007). This taxon is also enriched under fiber-deprived conditions in adult mice (Desai
64 *et al.*, 2016) and appears to have immunogenic properties when present in 14SM, including a high
65 IgA-coating index (Martens *et al.*, 2023). We sought to determine the role of this particular microbe
66 in early life development on the same FR diet by employing mice colonized with the full community
67 except *A. muciniphila* (13SM). By employing a longitudinal sampling approach among the pups of
68 each diet and SM combination, we isolated dietary and microbial drivers of early-life immune
69 development. We show that both the maternal diet and the presence or absence of *A. muciniphila*
70 are key contributing factors in shaping the host colonic transcriptome and the immune cell
71 populations during this critical early life window.
72

73 ## Results and discussion

74 *Gut microbiome colonization is shaped by maternal diet*

75 Consistent with previous reports (Earle *et al.*, 2015; Desai *et al.*, 2016), we observed an elevated
76 relative abundance of *Akkermansia muciniphila* in the parent mice fed a fiber-free (FF) diet compared
77 to those on a standard fiber-rich (FR) chow (**Dataset EV1**). We expected to observe similarly high
78 levels of *A. muciniphila* in the offspring of FF-fed dams; however, the expansion of *A. muciniphila*
79 was delayed among mice born to FF-fed dams (**Figs 1B–C**). This contrasts with the microbiome
80 development of 14SM FR pups, which showed strong initial colonization with *A. muciniphila* during
81 suckling, as anticipated given its ability to consume milk oligosaccharides (Kostopoulos *et al.*, 2020).
82 When mice began to consume a solid food diet between ages 15 to 20 days, the profiles rapidly
83 stabilized and resembled compositions observed in adult mice fed the respective diets (**Datasets**
84 **EV1–2**), as also verified by 16S rRNA gene sequencing (**Dataset EV3**). Among 14SM FF mice, *A.*
85 *muciniphila*, *Bacteroides caccae, Clostridium symbiosum*, and *Desulfovibrio piger* significantly
86 expanded to comprise approximately three-fourths of the microbiome composition. As *B. caccae* can
87 degrade complex polysaccharides and mucin, its elevated abundance on the FF diet may reflect a
88 functional shift towards increased mucin foraging, which can ultimately contribute to thinning of the
89 mucus barrier (Desai *et al.*, 2016) and promote production of immunostimulatory cytokines TNF and

90 IL-6 (Brown *et al.*, 2021). Although the consequences of an increase in *C. symbiosum* are less clear
91 from a functional standpoint, it is elevated in IBD and is an emerging biomarker for colorectal cancer
92 (Xie *et al.*, 2017). Similarly, *D. piger* may also contribute to development of local inflammation and
93 colorectal cancer via production of hydrogen sulfide (Blachier *et al.*, 2021), particularly when
94 combined with increased liberation of sulfate moieties by mucin-foraging bacteria under fiber-free
95 conditions.
96
97 Differences in the microbial assemblage between pups of 14SM and 13SM dams were less
98 pronounced than between pups from FR and FF-fed dams. However, we note a transient increase
99 in *Barnesiella intestinihominis*, a mucin-specialist, at day 25; *Collinsella aerofacians* at day 30, a
100 bacterium linked to increased gut permeability; and decrease in *Bacteroides ovatus* at day 20, a
101 bacterium linked to production of short-chain fatty acids and neuroactive compounds (Horvath *et al.*,
102 2022). After weaning, there was also a marked increase in *Marvinbryantia formatexigens*, an oligo-
103 saccharide degrading bacterium (Rey *et al.*, 2010) that can stimulate host IgA production via acetate
104 (Takeuchi *et al.*, 2021). Although preliminary, these data indicate that the absence of *A. muciniphila*
105 may have a distinct impact on the community structure and host immunity through diet-independent
106 mechanisms.
107
108 *Colonic transcriptome reflects differences in maternal diet*
109 *A. muciniphila* has been previously associated with regulation of host metabolic activity (Yoon *et al.*,
110 2021) and intestinal adaptive immunity in adult mice (Ansaldo *et al.*, 2019), but little is known about
111 its immune influence in early life. Therefore, to address the host physiological effects of this striking
112 difference in the abundance of *A. muciniphila* according to diet (**Fig 1**), we performed total RNA
113 sequencing on the distal colon tissues of 15 day-old pups born to FR and FF 14SM dams as well as
114 FR 13SM dams without *A. muciniphila* (**Fig 2, Fig EV1A, Dataset EV4**). Relative to the control group
115 (14SM FR), we detected changes in the expression level of 32 transcripts according to the maternal
116 diet (14SM FF) and 57 transcripts regulated by the presence of *A. muciniphila* (13SM FR) (**Fig 2A**

117 **top, Fig 2B, Dataset EV5–6**). Performing a gene set analysis based on Gene Ontology (GO) terms
118 for biological processes, we found differential enrichment according to the diet (14SM FR vs 14SM
119 FF), but not to the presence of *A. muciniphila* (14SM FR vs 13SM FR) (**Fig 2A bottom, Fig 2C**).
120 This may reflect two limitations of gene set analyses: 1) transcripts not corresponding to a common
121 pathway can still directly lead to changes in immune cell differentiation; and 2) transcripts
122 corresponding to pseudogenes or ncRNA may impact on host development through epigenetic
123 mechanisms or other undescribed pathways (**Fig EV1B, Dataset EV6**). Such cases would not be
124 highlighted in gene set analyses, therefore the absence of significant changes on the level of gene
125 sets for the 14SM FR vs 13SM FR comparison does not mean there are no biologically relevant
126 differences in the transcriptomes. For example, H2-K1 (a histo-compatibility gene involved in antigen
127 presentation), Gapdh (involved in glycolysis), and Gal3st2b (involved in glycosylation) represent
128 relevant differences between the 13SM and 14SM groups that can underlie the observed
129 immunological differences, but which do not correspond to a shared functional pathway (**Dataset**
130 **EV6**).
131
132 On a functional level, *Ppp3r2* and *Nlrp1b* led to the identification of the top 5 gene sets enriched in
133 14SM FR pups (**Fig 2C;** see **Dataset EV7** for all 29 gene sets), though less weight should be placed
134 on this finding since it was driven by only two genes. Comparing host transcriptomes according to
135 diet revealed an enrichment in transcripts involved in epithelial barrier development and cell–cell
136 adhesion (*Myh1*, *Myh8*, and *Myot*), as well as peptide cross-linking (*Sprr1a* and *F13a1*), anoikis or
137 apoptosis associated with cell detachment from the epithelial tissue (*Clca3a2* and *Itga5*), oxidative
138 stress-induced intrinsic apoptotic signaling pathways (*Hspb1* and *Nox1*), and response to interferon-
139 beta (*Tgtp2*, *Gbp2* and *Igtp*) among FF 14SM pups (**Fig 2B–C, Table EV7**). Some of these
140 transcripts, including *Nox1* (Szanto *et al.*, 2005), *Itga5* (Zhu *et al.*, 2021), and *Hspb1* (Arrigo *et al.*,
141 2007), are also implicated in colon cancer progression, suggesting potential pathological
142 development. The differential expression of these transcripts according to RNA sequencing was
143 further validated using primers specific to these transcripts. The RT-qPCR results exhibited a trend

144 consistent with expectations from RNA sequencing analyses, although these shifts were only
145 significant for *Nox1*, *Ppp3r2*, and *Ifit1bl1* (**Fig EV1D–E**). Several transcripts belonging to the
146 "response to interferon-beta" gene set were elevated among 14SM FF pups, however we detected
147 only a slight increase in *Ifnb1* among this group at 15 days of age that was not maintained at other
148 timepoints (**Fig EV1E**).
149
150 The postnatal period is critical for the development of the immune system as a weaning reaction to
151 colonizing microbes was shown to be protective against diseases in adulthood among mice
152 colonized with segmented filamentous bacteria (Al Nabhani *et al.*, 2019). Thus, in order to provide a
153 longitudinal element to the transcriptomic data, we performed RT-qPCR to quantify the relative
154 expression of transcripts corresponding to select cytokines involved in immunity and epithelial barrier
155 maintenance (**Fig 2D**). We noted an induction of *Infg* around 15 days among all groups, which is
156 considered characteristic of the weaning reaction. *Tnfa*, another marker of the weaning reaction,
157 was only elevated in the pups of 14SM fiber-deprived dams. By comparing transcript expression
158 levels to germ-free (GF) mice at age 15 days (**Fig 2D**), we see that some of the observed pro-
159 inflammatory shifts can be attributed to a combination of diet and microbiome composition. In
160 particular, at age 15 days, the FF diet increased the transcript levels of *Ifng*, *Il17f*, and *Il23* among
161 germ-free pups of fiber-deprived dams, relative to germ-free, fiber-rich-fed offspring (**Fig 2D, Fig**
162 **EV1C**). Although the expression of these cytokines is overall lower in germ-free conditions compared
163 to 13SM or 14SM, differences in the maternal diet may affect the baseline expression of these
164 cytokines in germ-free mice through a possibly different maternal milk composition. At the same age,
165 only pups of 14SM FF-fed dams displayed a strong elevation in *Tnfa* and *Il22* transcript levels,
166 reflecting compounding effects of the maternal diet and microbiome.
167
168 *Maternal fiber deprivation shapes microbiota-mediated immune development*
169 The transcript-level results underscore the potent impact of the maternal diet in shaping the
170 developing epithelial barrier and host immune system. Therefore, to confirm that these changes

171 translate into the profile of immune cell populations, we performed flow cytometry on cells isolated
172 from the colonic lamina propria (cLP) at age 15 days (**Fig 3, Fig EV2**). As an effect of colonization,
173 we observed elevated levels of cytotoxic NK cells and ILC3 among 14SM pups compared to GF
174 pups (**Fig 3A**), in agreement with previous reports comparing germ-free and colonized mice (Ganal
175 *et al.*, 2012; Sanos *et al.*, 2009). Consistent with the host transcriptomic data, maternal dietary fiber
176 intake appeared to play a role in immune cell profiles of both 14SM and GF pups. Particularly, pups
177 of 14SM FF dams had lower levels of ILC2 and higher levels of NCR^- ILC3 compared to pups of
178 14SM FR dams (**Fig 3A**). This aligns with observations by Babu et al. among pups of high-fat diet-
179 fed mothers, suggesting common underlying mechanisms driven by a Western-style diet (Babu *et*
180 *al.*, 2018). In the adaptive arm however, the 14SM colonization lowered the proportions of $CD8^+$ T
181 cells, $CD4^+$ T cells, Tregs and Th1 cells (**Fig 3B**). By contrast, Th17 cells were induced by the
182 colonization among pups of FR-fed dams but not fiber-deprived dams, suggesting that the maternal
183 dietary fiber intake differentially affects innate and adaptive $RORgt^+$ cells in the pup's colons.
184
185 Bacteria-derived metabolites represent a mechanistic link between changes in the microbiome and
186 host immunity. While it would be valuable to perform metabolomics analysis during this early life
187 period, we note that the overall volume of colonic contents available is a major limitation, especially
188 at 10–15 days of age. In the absence of such data, we would speculate that microbial metabolism
189 of tryptophan, which is abundant in milk, may drive many of the observed microbiota-mediated
190 immune changes. Microbial or host degradation of dietary tryptophan yields indole derivatives which
191 can function as AhR ligands and stimulate production of IL-22 from ILC3s (Qiu *et al.*, 2012; Li *et al.*,
192 2018), both of which were elevated among pups of 14SM FF-fed dams at 15 days of age (**Fig 2D,**
193 **3A**). The expansion of these innate subsets also leads to apoptosis of commensal-specific CD4+
194 and CD8+ T cells (Hepworth *et al.*, 2015; Liu *et al.*, 2019). Likewise, among adaptive cell subsets,
195 Th17 cells were significantly elevated among 14SM FR mice, potentially reflecting the effects of
196 increased colonization with *A. muciniphila* in early life, since this bacterium can act as a direct AhR
197 ligand via its outer membrane protein Amuc_1100 (Gu *et al.*, 2021). Finally, we note that a fixed

198 number of cells were stained per organ, therefore the higher proportions of adaptive cell subsets
199 (namely $CD8^+$, $CD4^+$, Tregs, and Th1 cells) observed in GF mice may simply reflect a lower absolute
200 number of innate cells (Macpherson and Harris, 2004; Kennedy *et al.*, 2018).
201
202 Akkermansia muciniphila *alters innate and adaptive immunity in early life*
203 To determine the role of *A. muciniphila* in the aforementioned colonization effect, we compared the
204 immune cell profiles of pups born to FR-fed 14SM, 13SM and GF dams (**Fig 3**). Under FR conditions,
205 colonization differentially affected the proportions of innate cell subsets, with ILC3s favored under
206 14SM conditions (p=0.0023) versus ILC2 cells under 13SM conditions (p=0.0400) (**Fig 3A**). Although
207 the FF diet skewed toward ILC2 in the absence of a microbiota, the strong enrichment of ILC3s in
208 14SM colonized mice (p=0.004) led to a null effect when comparing ILC2 proportions in pups of
209 14SM and GF FF-fed dams directly. These results highlight the complex interactions between diet
210 and microbiota on immune development in early life.
211
212 Interestingly, an increase of NCR^- ILC3 and Th17, and the decrease of $CD8^+$ T cells, $CD4^+$ T cells,
213 Tregs and Th1 cells in pups born to 14SM FR-fed dams, relative to those of GF FR-fed dams, was
214 not observed in pups born to 13SM dams, confirming a specific impact of *A. muciniphila* on these
215 immune cell populations. Furthermore, only Th17 cells were decreased in pups born to 14SM FF-
216 fed dams, consistent with a reduced relative abundance of *A. muciniphila* at this time point compared
217 to pups born to 14SM FF-fed dams (**Fig 3B**). These results support an early life induction of the
218 colonic Th17 population that is driven by the maternal dietary fiber intake and mediated locally by *A.*
219 *muciniphila* in the pups colons. Th17 cells play a key role in progression of multiple sclerosis, an
220 autoimmune disease that has also been correlatively linked to presence of *A. muciniphila* in patients
221 (Jangi *et al.*, 2016) and mechanistically in mouse models of multiple sclerosis (Lin *et al.*, 2021).
222 Although the precise nature of the link between *Akkermansia* and exacerbation of autoimmune
223 encephalomyelitis has not yet been shown (e.g. MAMP recognition, physiological alterations from

224 mucin-degrading activities), this relationship bears further investigation to identify potential
225 therapeutic targets.
226

227 **Conclusion**

228 Summarizing these findings, we demonstrate: 1) that the maternal diet alters the host colonic
229 transcriptomic and immune profile among pups during the weaning period; and 2) that these
230 observed alterations can also be tuned by the inclusion or exclusion of a single bacterium from a
231 defined community (**Fig 4**). The mechanisms behind such immunomodulatory effects can be via
232 microbial metabolites such as SCFA or AhR ligands, or via surface molecules such as LPS (Davis
233 *et al.*, 2022). In the latter instance, Kostopoulos et al. demonstrated that *A. muciniphila* produces
234 more immune-regulatory pili-protein when grown on human milk, highlighting diet-dependent factors
235 that can indirectly strengthen barrier integrity via the microbiome (Kostopoulos *et al.*, 2020). In line
236 with this, we found that presence of *A. muciniphila* skews toward a type 3 response, whereas its
237 absence appears to favor a type 1 or 2 response. Overall, our results highlight the importance of the
238 maternal microbiome composition and dietary fiber intake in postnatal microbiome maturation and
239 immune development, which could have implications for development of various immune-mediated
240 diseases later in life.
241

242 In this study, we assessed the compounding effects of a fiber-free diet across generations with mice
243 pups weaned onto the same diet as the dams. While the observed immune changes occur prior to
244 weaning, modifying the diet at distinct developmental stages (in utero, pre-weaning, and post
245 weaning) would provide insights into critical key drivers of early life immune development.
246 Furthermore, it would be of interest to interrogate both the persistence of the observed differences
247 in early life immunity in an adult mouse and the effects of this differential development in a relevant
248 disease model (**Fig 4**). For example, Al Nababi et al. showed that the weaning reaction provided
249 protection against oxazolone-induced colitis—a type-2 inflammation—and, considering the
250 enrichment type 2 immune cell subsets in pups of 13SM FR-fed mice at 15 days of age, this could

251 be an promising model to further investigate diet and microbiota effects on immunity at distinct
252 developmental stages. Thorburn et al., for example, found that fiber supplementation during
253 pregnancy alone was sufficient to prevent asthma development in offspring (Thorburn *et al.*, 2015).
254 Although the involvement of the microbiome was not explored by Thorburn et al., we previously
255 documented the synergistic impact of diet and *A. muciniphila* in the context of food allergy (Parrish,
256 Boudaud, *et al.*, 2022). However, the study by Parrish et al. was performed in adult mice that were
257 colonized by oral gavage, therefore the question remains as to how exposure to *A. muciniphila* in
258 early life might play into the development and severity of allergic responses. Finally, mouse models
259 of multiple sclerosis might also be of interest considering RORgt+ immune cell subsets were strongly
260 affected by the maternal diet or microbiome changes in the present study and this same subset is
261 also known to drive the demyelination that characterizes this disease.
262
263 Additionally, future studies should characterize the maternal milk components to improve
264 understanding of the mechanisms for *A. muciniphila* suppression, which occurred only in pups born
265 to fiber-deprived dams. As illustrated in **Fig 4**, a potential explanation for this phenomenon includes
266 changes in quantity or specificity of IgG—the dominant maternal antibody transferred via murine
267 breast milk (Zheng *et al.*, 2020)—which can be also specifically induced by *A. muciniphila* (Ansaldo
268 *et al.*, 2019). Follow-up studies should be performed to investigate whether increased *A. muciniphila*
269 and mucus erosion among FF-fed dams facilitates immune recognition of this bacterium, leading to
270 increased the production of specific-IgG in breastmilk, ultimately preventing *A. muciniphila*
271 colonization and Th17 induction among offspring in early life. Another explanation for *A. muciniphila*
272 suppression may be related to differences in the types of linkages presented by the milk
273 oligosaccharides, which could hamper their effective utilization by *A. muciniphila.* To this point,
274 Kostopoulos et al. demonstrated that *A. muciniphila* can degrade 2'-fucosyllactose, lacto-N-tetraose,
275 lacto-N-triose II, lactose, and 3'-sialyllactoses (Kostopoulos *et al.*, 2020), although it also bears
276 mentioning that these structures are common components of human milk, which is expected to have
277 a slightly different compositional and structural makeup compared to murine milk (Luna *et al.*, 2022).

Improved understanding of these milk-associated mechanisms in both humans and rodent models are warranted, as these insights could provide tools to augment growth or activity of *A. muciniphila* in various disease contexts.

While the 14SM model enables controlled investigation of the effects the microbiome on host immune development, it is important to note that the 14SM consortium is based on an adult human colonic microbiome. Although the species in this community are closely related to strains that are normally found in the mouse gut and thus readily colonise upon oral gavage in germ-free mice (Desai *et al.*, 2016), the 14SM lacks certain members, such as bifidobacteria and lactobacilli, which are abundant in early life and mostly colonize the small intestine. These members could be added to the community in future studies, however we would also highlight that a community strictly designed to model the pre-weaning mouse gut would present its own set of limitations. To this point, Lubin et al. demonstrated that restricting the microbiome to a pre-weaning community halts immune development and increases susceptibility to *Salmonella* infection (Lubin *et al.*, 2023), reflecting the need for a functionally-balanced synthetic community to elicit normal immune development. As with other gnotobiotic models, the 14SM immune profiles typically represent an intermediate between germ-free and SPF colonization states in adulthood, potentially due to low diversity, low bacterial density and/or absence of specific immunogenic bacteria such as segmented fillamentous bacteria (Parrish, Grant, *et al.*, 2022). Addition of new members may be a promising approach to refine these models, although it remains difficult to completely recapitulate SPF immune profiles (Afrizal *et al.*, 2022). Despite these limitations, synthetic microbiota models remain critical tools to dissect specific interactions between the microbiome and diet in early life.

This work highlights numerous underexplored factors related to the potential for maternal fiber deprivation to alter postnatal establishment of mucin-degrading gut bacteria and immune maturation. The elevated levels of RORgt-induced innate and adaptive cell subsets among *A. muciniphila*-colonized mice is important for preventing translocation of gut microbes into the host (De Agüero *et*

305 *al.*, 2016) and can also be associated with protection against chronic inflammation via TLR4 (Liu *et*
306 *al.*, 2022). Considering *A. muciniphila* is only found in approximately half of the human population
307 (Geerlings *et al.*, 2018), linking this bacterium to exacerbation or amelioration of specific gut-linked
308 diseases is particularly interesting as it highlights its potential as a biomarker for disease risk.
309 Although *A. muciniphila* has been proposed as a probiotic (Cheng and Xie, 2021), mainly due to its
310 strong benefits in countering metabolic diseases, the various conflicting reports involving this
311 bacterium and health, as discussed by Cirstea et al. (Cirstea *et al.*, 2018), caution against premature
312 generalizations and underscore the need to consider factors such as diet and underlying disease
313 context. Ultimately, insights provided by the present study and follow-up works are expected to hold
314 translational relevance in improving human health outcomes as modern lifestyle practices (e.g.
315 antibiotics use, Western-style diets) contribute to perturbation of the gut microbiota and immune
316 function across generations (Sonnenburg *et al.*, 2016) and in early life (Robertson *et al.*, 2019).
317

318 ## Materials and Methods

319 ### Mice

320 All experimental procedures involving animals (i.e. initial gavage of parental mice) were approved
321 by the Luxembourgish Ministry of Agriculture, Viticulture and Rural Development (LUPA 2019/49).
322 Mouse work was performed according to the "Règlement grand-ducal du 11 janvier 2013 relatif à la
323 protection des animaux utilisés à des fins scientifiques" based on the "Directive 2010/63/EU" on the
324 protection of animals used for scientific purposes. Mice were housed in the germ-free facility of the
325 University of Luxembourg in either colonization-specific isolators or individually ventilated cages.
326 Germ-free Swiss Webster mice were orally gavaged with 13SM or 14SM at 6–8 weeks of age.
327 Gnotobiotic mice and germ-free (GF) controls were fed the respective diets for at least 20 days prior
328 to start of breeding. There was no significant difference in litter sizes between the 5 groups (13SM
329 FR, 14SM FR, 14SM FF, GF FR, GF FF), however we did observe transient differences in pup
330 weights according to diet and colonisation during weaning (**Fig EV3**). At 3 weeks of age, pups were
331 weaned (i.e. physically separated from dams) and provided the same diet as the dams. Blinding was

332 not possible as the colonization dictated the order of mouse handling and the diets are visually
333 distinct.
334
335 **Diet formulation and administration**
336 All parental mice were maintained on the FR diet, which is a standard rodent chow (SAFE®R04,
337 Augy, France), until 2 weeks after the oral gavage. After this period, the parental mice designated
338 as FF were switched to the custom fiber-free chow, which is a modified version of Harlan TD.08810
339 diet and is manufactured by the same vendor as the FR diet, as previously reported (Parrish, Grant,
340 *et al.*, 2022). Mice were maintained on the FF diet for at least 20 days prior to setting breeding pairs
341 and the respective diets were administered *ad libitum* for the remainder of the study.
342
343 **Bacterial culturing and colonization of 13- or 14-member synthetic microbiota (SM)**
344 Culturing and colonization of GF mice with the 13- or 14-member synthetic microbiota (SM) was
345 performed as previously described (Steimle *et al.*, 2021). The 14SM community contains the
346 following bacteria (all type strains, unless otherwise indicated): *Akkermansia muciniphila*, *Collinsella*
347 *aerofaciens*, *Desulfovibrio piger*, *Escherichia coli* HS, *Faecalibacterium prausnitzii* A2-165,
348 *Roseburia intestinalis*, *Marvinbryantia formatexigens*, *Clostridium symbiosum*, *Eubacterium rectale*
349 A1-86, *Barnesiella intestinihominis*, *Bacteroides caccae*, *Bacteroides uniformis*, *Bacteroides ovatus*,
350 and *Bacteroides thetaiotaomicron*. The 13SM mice were orally gavaged with the same strains with
351 the exception of *A. muciniphila*. Bacterial colonization among the parental mice was verified by qPCR
352 of fecal DNA at 7 days post-oral gavage using strain-specific primers. Note that *R. intestinalis* and
353 *E. rectale* did not consistently transfer to the pups during the early life period, despite being detected
354 in the parents.
355
356 **Tissue processing**
357 Distal colons were washed in PBS to collect contents, then transferred to 1 ml RNAprotect Tissue
358 Reagent (Qiagen, Hilden, Germany) for colonic transcript analyses. Tissues were held in RNAprotect

359 at 4°C for 2 days, after which the reagent was removed and the tissues stored at –80°C. For mice
360 that would undergo FACS analyses, the entire colon was transferred into ice-cold 3 ml Hank's
361 balanced salt solution (HBSS) containing 10 mM HEPES and without Ca^{2+} and Mg^{2+}. Cells from the
362 colonic lamina propria (cLP) were isolated using a Lamina Propria Dissociation Kit (Miltenyi Biotec,
363 Bergisch Gladbach, Germany) on the gentleMACS Dissociator (Miltenyi Biotec), following the
364 manufacturer's instructions. Cells were washed, counted, and re-suspended in FACS buffer (PBS;
365 1% FCS; 5mM EDTA) until cell staining.
366
367 **Flow cytometry**
368 A total of 1.5×10^6 cells per animal were transferred into a U-bottom 96-well plate for staining. For
369 live/dead staining, cells were incubated in 100 µl PBS 1X containing 1.5 µL Zombie NIR Fixable
370 Viability kit (BioLegend, San Diego, CA, USA) at 4°C for 30 min. Cells were washed twice using
371 FACS buffer and subsequently fixed with the FoxP3 Fix/Perm kit (eBiosciences, Uithoorn,
372 Netherlands) for 45 min at 4°C, followed by permeabilization wash. Purified Rat Anti-Mouse
373 CD16/CD32 (Mouse BD Fc Block™, BD Biosciences, San Jose, CA, USA) was added at a
374 concentration of 1 µg per 10^6 cells, incubated at 4°C for 30 min, then cells were washed twice in
375 permeabilization buffer. Cells were stained with anti-CD4 BV605 (#100548, clone RM4-5, 1:700,
376 Biolegend), anti-CD3 BV711 (#100241, clone 17A2, 1:88, Biolegend), anti-CD45 BV780 (#564225,
377 clone 30-F11, 1:88, BD), anti-CD335/NKp46 FITC (#137606, clone 29A1.4, 1:100, Biolegend), anti-
378 CD8 PE-Cy5 (#100710, clone 53-6.7, 1:700, Biolegend), anti-FoxP3 eF450 (#48-5773-82, clone
379 FJK-16s, 1:200, eBiosciences), anti-GATA3 PE (#100710, clone 53-6.7, 1:44, Biolegend), anti-
380 EOMES PE-eF610 (#61-4875-82, clone Dan11mag, 1:100, eBiosciences), anti-Tbet PE-Cy7
381 (#644824, clone 4B10, 1:44, Biolegend), and anti-RORgt APC (#17-6988-82, clone AFKJS-9, 1:22,
382 eBiosciences). Cells were incubated with the staining mix for 30 min at 4°C, then washed twice with
383 FACS buffer. Samples were acquired on a NovoCyte Quanteon flow cytometer (ACEA Biosciences
384 Inc., San Diego, CA, USA). Raw fcs files were analyzed in FlowJo version 10.8.1, with innate cell
385 populations gated as described by Burrows et al. (Burrows *et al.*, 2020). An example of the gating

386 strategy is illustrated in **Fig EV2**. The dataset was exported as a percent of the total $CD45^+$ cells for
387 subsequent statistical analyses.
388
389 **DNA extraction and microbiome compositional analyses**
390 Distal colon contents were collected by opening the colon longitudinally and washing tissue in 1 ml
391 PBS. The PBS and contents were then centrifuged at 10 000 g for 10 min and the PBS supernatant
392 was removed. Pelleted contents were stored at –20°C until DNA extraction using the phenol-
393 chloroform method, as described by Steimle et al. (Steimle *et al.*, 2021). The concentration of DNA
394 was measured using a NanoPhotometer N60 (Implen, Munich, Germany). The purified DNA was
395 diluted to 20 ng/ul and then subjected to qPCR with primers specific to each of the 14 bacterial
396 strains, as previously described (Steimle *et al.*, 2021). As the primers are specific to each strain and
397 the target sequence is present only once in the respective genome (Desai *et al.*, 2016), this method
398 was used to allow for estimation of the number of each individual bacterial genomes or the absolute
399 abundance of bacteria in the contents of the distal colon (**Dataset EV1–2**). As tissues were washed
400 in 1X PBS to collect the contents, this estimation is based on the total contents, not normalized by
401 the content weight, and can therefore vary according to factors such as mouse age, diet, and recent
402 defecation. Streamplots based on the average abundance at each time point were created in
403 Microsoft Excel 2016. In order to rule out contamination with non-14SM strains, we also performed
404 16S sequencing on a subset of samples. For this method, DNA concentration was assessed using
405 the Qubit® dsDNA HS assay kit on a Qubit® 3.0 fluorometer (Life Technologies, Eugene, Oregon,
406 USA). To rule out contamination with non-14SM members, sequencing of the V4 region of the 16S
407 rRNA gene was carried out on an Illumina MiSeq system at the Integrated BioBank of Luxembourg
408 (IBBL, Dudelange, Luxembourg), as previously described by Neumann et al. (Neumann *et al.*, 2021).
409 Note that 16S rRNA sequencing data is not well suited for analysis of 14SM because it cannot
410 distinguish the three *Bacteroides* species well and because the variations in copy number can lead
411 to biases in relative abundance calculations, nonetheless the results from the two methods are well-
412 correlated for most of the SM strains (**Fig EV4**). Raw fastq sequences were processed via QIIME2

413 version 2020.6 (Bolyen *et al.*, 2019) using DADA2 (Callahan *et al.*, 2016) for quality control.
414 Taxonomic assignment was carried out with the SILVA 138 database (Quast *et al.*, 2013) (**Dataset**
415 **EV3**).
416
417 **RNA extraction**
418 Distal colon tissues were stored at –80°C until RNA extraction. Tissues were incubated overnight at
419 –80°C in 1 ml TRIzol™ Reagent (Life Technologies Europe BV, Bleiswijk, Netherlands). A 5mm
420 autoclaved metal bead was added to the sample, followed by homogenization on a RETSCH Mixer
421 Mill MM 400 for 5 min at 30 Hz. Samples were centrifuged at 4°C for 5 min at 12 000 × g. The
422 supernatant was transferred to a new tube and incubated for 5 min at room temperature. For each
423 sample, 200 µl pure chloroform was added, then mixed by shaking for 15 s and incubated at room
424 temperature for 3 min. Next, samples were centrifuged for 15 min at 4°C, 12 000 × g, and the
425 aqueous phase was recovered. A volume of 500 µl isopropanol was added, followed by vigorous
426 mixing and incubation at room temperature for 10 min. Samples were centrifuged at the same
427 settings as previously. Then, the pellet was recovered and washed in 1 ml ice-cold 75% ethanol and
428 vortexed briefly before centrifugation at 4°C for 5 min at 7 500 × g. The supernatant was discarded
429 and the pellets were air-dried for 10 min at 37°C before re-suspending in 50 µl Invitrogen™
430 UltraPure™ DNase/RNase-free distilled water (Life Technologies Europe BV, Bleiswijk,
431 Netherlands). The RNA solution was further incubated for 15 min at 56°C to fully re-suspend the
432 pellet. DNase treatment to remove genomic DNA was done by adding 2 µl DNAse I (1 U/µl), 10 µl
433 DNase I Buffer (10X), plus 40 µl water for 30 min at 37°C. Next, 1 µl of 0.5M EDTA was added to
434 each sample and the DNAse I was inactivated by heating at 65°C for 10 min. RNA purification was
435 performed with the RNeasy mini kit (QIAGEN Benelux BV, Venlo, Netherlands) according to
436 manufacturer's instructions. RNA was eluted in Invitrogen™ UltraPure™ DNase/RNase-free distilled
437 water (Life Technologies Europe BV, Bleiswijk, Netherlands) and stored at –80°C.
438
439 **RT-qPCR**

440 Complementary DNA libraries were prepared from 200 ng purified RNA in 11 µl water, 1 µl 2.5 uM
441 random primers and µl 500 uM dNTPs (Life Technologies Europe BV, Bleiswijk, Netherlands),
442 heated to 65°C for 5 min (lid temperature 112°C), then incubated at 4°C for at least 1 min. Afterwards,
443 1x SSIV buffer, 1 µl DTT, 1 uL RNaseOUT, and 1 uL SuperScript™ IV Reverse Transcriptase (Life
444 Technologies Europe BV, Bleiswijk, Netherlands) was added to each tube. Samples were held at
445 23°C for 10 min, then 50°C for 10 min, and finally heated to 80°C for 10 min to inactivate enzymes.
446 Quantitative PCR was carried out according to standard protocols, briefly: 1 ul of template cDNA
447 was mixed with 8.7 µl water,1.2 µl 1x buffer, 0.625 µl 2.5 mM MgCl2, 0.5 µl 400uM dNTPs, 0.1 µl
448 each of 0.2 uM forward and reverse primers (**Table 1**), 0.125 µl 1x SYBR green fluorescent dye, and
449 0.1 µl 0.5 U Taq DNA polymerase (Life Technologies Europe BV, Bleiswijk, Netherlands). Samples
450 were pre-denatured at 94°C for 5 min; then underwent 40 cycles at 94°C for 20 s, 60°C for 50 s,
451 72°C for 45 s. Finally, samples were maintained at 72°C for 5 min and the melting curve was
452 generated over 15 s by heating from 65°C–95°C at 0.3°C increments. Colonic transcript expression
453 levels were normalized to levels of *Hprt*, which was identified as the most stable housekeeping gene
454 over time and conditions using RefFinder (http://blooge.cn/RefFinder), in comparison to *Gapdh* and
455 *Hsp90* (**Dataset EV8**).
456

Table 1. Primers for RT-qPCR against colonic cDNA transcript library

Target	Sequence FW	Sequence RV
	5' to 3'	
Ifng	GCACAGTCATTGAAAGCCTA	GCTTCCTGAGGCTGGATT
Tnfa	AGCCCACGTCGTAGCAAAC	GATAGCAAATCGGCTGACGG
Il17f	GGTAGCAGCTCGGAAGAACC	TGGAATTCACGTGGGACAGA
Il22	TCGTCAACCGCACCTTTATG	CCCGATGAGCCGGACA
Il12p40	TGTGGAATGGCGTCTCTGTC	GCCTTTGCATTGGACTTCGG
Il23	TGGAGCAACTTCACACCTCC	GGGCAGCTATGGCCAAAAAG
Hprt	GTTGGGCTTACCTCACTGCT	TAATCACGACGCTGGGACTG
Hsp90	CAGAAGGCTGAGGCAGACAA	ATCATGCGGTAGATGCGGTT
Gapdh	AATTCAACGGCACAGTCAAGGC	GTGGTTCACACCCATCACAAA
Ifnb1	GTCCTCAACTGCTCTCCACT	CATCCAGGCGTAGCTGTTGTA
Fos	GGTTTCAACGCCGACTACGA	GCGCAAAAGTCCTGTGTGTT
Tgtp2	GCCCACAAGCGTCACGTATT	GCTATGGCATCATTGGCTGC
Igtp	AGCCCGTCTTTTCACGACTT	TGCACTTGTCGCAGACTTGA
Gbp2	AGCTGCACTATGTGACGGAG	TAGCGGAATCGTCTACCCCA

Itga5	CCGGGAAGGGACGGAGTC	CCCACAGCCACAGAGTATCC
Clca3a2	AGTGCGTGTCCAGGCAAGA	GCACCCAGTGCAGAGATACT
F13a1	GTCCCGCCCAATAACTCCAA	CCCTCTGCGGACAATCAACT
Nox1	GGCCATGGATGGATCTCTCG	TGCCTGCAACTCCCCTTATG
Hspb2	CTGCCGAGTACGAATTTGCC	TGATAGAGGGTGGGGGTCAG
Ppp3r2	ACCAAACTGAGCTGTGCAAC	CATCACCCTTGACGCTGAAC
Nlrp1b	TTGTGGCTTGTTGAATGCGG	AGCTGCAGGTCTAGCTCTCT
Ifit1bl1	AAGGCTCTGAAAGTGGAGCC	CCAAAGACATAGGGCTGCGA

RNA sequencing and analysis

RNA integrity (RIN) was determined using a 2100 Bioanalyzer RNA Nanochip (Agilent, Santa Clara, CA, USA). Samples selected for RNA sequencing had RIN values ranging from 7.7–9.8. RNA libraries were prepared using an Illumina® Stranded Total RNA Prep kit, along with Ribo-Zero Plus to deplete ribosomal RNA. Samples were then sequenced in a 2 × 75 bp arrangement with a High Output Flow Cell on an Illumina NextSeq 550 system (Illumina, San Diego, CA, USA) at the LuxGen sequencing platform (Dudelange, Luxembourg). Adapters were removed using Cutadapt (Martin, 2011), followed by reads mapping and enumeration of gene counts with STAR 2.7.9a (Dobin *et al.*, 2013) (**Dataset EV4**). Transcripts that did not appear at least one time on average across all samples were filtered from downstream analyses. Two outliers were identified based on variation on PC1 of the top 500 most variable genes and excluded from subsequent analyses (**Fig EV1A**). Samples normalization was performed using the median of ratios method, followed by differential expression analysis in R using DESeq2 1.30.1 (Love *et al.*, 2014). Default parameters were used and *p* values were adjusted according to the Benjamini-Hochberg method. Differential expression was considered significant based on an adjusted *p* value<0.05. Differential expression analysis was performed for pairwise comparisons 14SM FF vs 14SM FR (**Dataset EV5**) and 14SM FR vs 13SM FR (**Dataset EV6**) (Love *et al.*, 2014). Gene set analysis was also carried out in R using the clusterProfiler 3.18.1 enrichGO function (Yu *et al.*, 2012) to identify up- or downregulated gene sets according to Gene Ontology (GO) terms (**Dataset EV7**).

Statistical analysis

Unless otherwise specified, statistical analyses were carried out using GraphPad Prism version 9.3.1 for Windows (GraphPad Software, San Diego, CA, USA). For mRNA expression data by RT-qPCR, values were log-transformed prior to statistical analyses by one-way ANOVA and residuals tested for normality by the Kolmogorov-Smirnov test. For FACS data, outliers were identified in GraphPad using the ROUT method (Q = 10%), followed by a one-way ANOVA was used with multiple comparison correction using the Benjamini-Hochberg method. Only biologically-relevant pairwise statistical comparisons are shown on the plots: 13SM FR vs. 14SM FR, 13SM FR vs. GF FR, 14SM FR vs. 14SM FF, 14SM FR vs. GF FR, 14SM FF vs. GF FF, and GF FR vs. GF FF. Data are from independent experiments (pups born from up to 4 litters derived from 2–3 breeding pairs per condition) and represent biological replicates.

Data Availability

The datasets produced in this study are available in the following databases:

- RNA-Seq and 16S rDNA data: European Nucleotide Archive (ENA) at EMBL-EBI PRJEB55622 (https://www.ebi.ac.uk/ena/browser/view/PRJEB55622)
- Flow cytometry data: FlowRepository (Spidlen *et al.*, 2012) FR-FCM-Z5X6 (https://flowrepository.org/id/FR-FCM-Z5X6)

Acknowledgements

Figure 4 was made using BioRender (Biorender.com). We thank the Luxembourg National Research Fund (FNR) for funding this research through CORE grants (C15/BM/10318186 and C18/BM/12585940) to M.S.D.; E.T.G. was supported by the FNR PRIDE (17/11823097) and the Fondation du Pélican de Mie et Pierre Hippert-Faber, under the aegis of the Fondation de Luxembourg; M.B. was supported by a European Commission Horizon 2020 Marie Skłodowska-Curie Actions individual fellowship (897408). We acknowledge the National Cytometry Platform (NCP) for assistance with generating flow cytometry data. The NCP is supported by Luxembourg's Ministry of Higher Education and Research (MESR) funding.

Author contributions

Erica T Grant: Conceptualization, data curation, formal analysis, investigation, methodology, software, validation, visualization, writing – original draft, writing – review & editing. **Marie Boudaud**: Conceptualization, data curation, formal analysis, investigation, methodology, validation, visualization, writing – review & editing. **Arnaud Muller**: Data curation, formal analysis, software, writing – review & editing. **Andrew J Macpherson**: Resources, writing – review & editing. **Mahesh S Desai**: Conceptualization, funding acquisition, investigation, methodology, project administration, resources, supervision, writing – review & editing

Conflict of interest

Mahesh S. Desai works as a consultant and an advisory board member at Theralution GmbH, Germany.

The Paper Explained

PROBLEM

There is a growing awareness that the early life period is a critical window for shaping the course of neonatal development and future health outcomes. However, little is known regarding the effects of maternal diet and microbiome composition on the interconnected establishment of the gut microbiome and host immunity in the progeny. We sought to understand the role of maternal dietary fiber intake on early life development by breeding mice colonized with a 14-member synthetic microbiota (SM), fed a fiber-deficient diet. We further investigated the effects of discrete changes in the maternal microbiome by colonizing a third breeding pair with the full SM except *Akkermansia muciniphila*, a somewhat controversial, health-associated commensal that can digest milk oligosaccharides and host mucins.

RESULTS

533 Pups born to dams fed a standard, fiber-rich chow showed initial colonization with *A. muciniphila*,
534 followed by an expansion of fiber-degrading bacteria upon switching to solid food. Conversely,
535 among pups of dams fed a fiber-free diet, *A. muciniphila* did not proliferate until after weaning,
536 suggesting that maternal milk factors influenced by diet shape pups' microbiome development. Pups
537 of fiber-deprived dams expressed a significantly higher quantity of colonic tissue transcripts
538 corresponding to defense response pathways against external antigens, and harbored lower
539 proportions of group 2 innate lymphoid cells and Th17 cells. Pups of fiber-rich-fed mice lacking *A.*
540 *muciniphila* demonstrated reduced proportions of innate and adaptive RORγt-positive immune cell
541 subsets.

542 IMPACT

543 The link between *A. muciniphila* and RORγt-positive immune cell subsets represents an intriguing
544 potential to alter immunity by targeting a single bacterium, however the mechanisms underlying this
545 interaction warrant further investigation. The unexpected suppression of *Akkermansia* among pups
546 of fiber-free fed dams during the weaning period encourages the characterization of maternal milk
547 components that might be used to support or limit growth of certain bacteria during early life. Using
548 a tractable gnotobiotic mouse model and custom diet, we highlight the powerful potential to
549 manipulate the microbiome and immunity during early life, which may have important implications
550 for prevention of modern diseases such as allergy and autoimmunity.

551

552 **For more information**

553 Gene Ontology (GO) Resource: http://geneontology.org/

554 RefFinder: http://blooge.cn/RefFinder/

555 Eco-Immunology and Microbiome Group (EIM): https://eim.lih.lu

556 Luxembourg Genome Center (LuxGen): https://luxgen.lih.lu

557 Luxembourg Institute of Health Research Portal: https://researchportal.lih.lu/

558 **References**

559 Afrizal A, Jennings SA V, Hitch TCA, Riedel T, Basic M, *et al.* (2022) Enhanced cultured diversity of
560 the mouse gut microbiota enables custom-made synthetic communities. *Cell Host Microbe* **30**
561 (11), 1630–1645.

562 De Agüero MG, Ganal-Vonarburg SC, Fuhrer T, Rupp S, Uchimura Y, *et al.* (2016) The maternal
563 microbiota drives early postnatal innate immune development. *Science.* **351** (6279), 1296–
564 1302.

565 Ansaldo E, Slayden LC, Ching KL, Koch MA, Wolf NK, *et al.* (2019) Akkermansia muciniphila induces
566 intestinal adaptive immune responses during homeostasis. *Science.* **364** (6446), 1179–1184.

567 Arrigo A-P, Simon S, Gibert B, Kretz-Remy C, Nivon M, *et al.* (2007) Hsp27 (HspB1) and αB-
568 crystallin (HspB5) as therapeutic targets. *FEBS Lett.* **581** (19), 3665–3674.

569 Babu ST, Niu X, Raetz M, Savani RC, Hooper L V, *et al.* (2018) Maternal high-fat diet results in
570 microbiota-dependent expansion of ILC3s in mice offspring. *JCI insight* **3** (19)

571 Blachier F, Andriamihaja M, Larraufie P, Ahn E, Lan A, *et al.* (2021) Production of hydrogen sulfide
572 by the intestinal microbiota and epithelial cells and consequences for the colonic and rectal
573 mucosa. *Am. J. Physiol. Liver Physiol.* **320** (2), G125–G135.

574 Bolyen E, Rideout JR, Dillon MR, Bokulich NA, Abnet CC, *et al.* (2019) Reproducible, interactive,
575 scalable and extensible microbiome data science using QIIME 2. *Nat. Biotechnol.*

576 Brown RL, Larkinson MLY, and Clarke TB (2021) Immunological design of commensal communities
577 to treat intestinal infection and inflammation. *PLoS Pathog.* **17** (1), e1009191.

578 Burrows K, Chiaranunt P, Ngai L, and Mortha A (2020) Rapid isolation of mouse ILCs from murine
579 intestinal tissues. In: *Methods in Enzymology*. Elsevier, Vol631,pp. 305–327

580 Callahan BJ, McMurdie PJ, Rosen MJ, Han AW, Johnson AJA, *et al.* (2016) DADA2: High-resolution
581 sample inference from Illumina amplicon data. *Nat. Methods* **13** (7), 581–583.

582 Cheng D and Xie MZ (2021) A review of a potential and promising probiotic candidate—Akkermansia
583 muciniphila. *J. Appl. Microbiol.* **130** (6), 1813–1822.

584 Cirstea M, Radisavljevic N, and Finlay BB (2018) Good bug, bad bug: breaking through microbial

585 stereotypes. *Cell Host Microbe* **23** (1), 10–13.

586 Collado MC, Derrien M, Isolauri E, de Vos WM, and Salminen S (2007) Intestinal integrity and
587 Akkermansia muciniphila, a mucin-degrading member of the intestinal microbiota present in
588 infants, adults, and the elderly. *Appl. Environ. Microbiol.* **73** (23), 7767–7770.

589 Davis EC, Castagna VP, Sela DA, Hillard MA, Lindberg S, *et al.* (2022) Gut microbiome and breast-
590 feeding: Implications for early immune development. *J. Allergy Clin. Immunol.* **150** (3), 523–
591 534.

592 Desai MS, Seekatz AM, Koropatkin NM, Kamada N, Hickey CA, *et al.* (2016) A Dietary Fiber-
593 Deprived Gut Microbiota Degrades the Colonic Mucus Barrier and Enhances Pathogen
594 Susceptibility. *Cell* **167** (5), 1339-1353.e21.

595 Dobin A, Davis CA, Schlesinger F, Drenkow J, Zaleski C, *et al.* (2013) STAR: ultrafast universal
596 RNA-seq aligner. *Bioinformatics* **29** (1), 15–21.

597 Earle KA, Billings G, Sigal M, Lichtman JS, Hansson GC, *et al.* (2015) Quantitative Imaging of Gut
598 Microbiota Spatial Organization. *Cell Host Microbe* **18** (4), 478–488.

599 Ganal SC, Sanos SL, Kallfass C, Oberle K, Johner C, *et al.* (2012) Priming of natural killer cells by
600 nonmucosal mononuclear phagocytes requires instructive signals from commensal microbiota.
601 *Immunity* **37** (1), 171–186.

602 Geerlings SY, Kostopoulos I, De Vos WM, and Belzer C (2018) Akkermansia muciniphila in the
603 human gastrointestinal tract: when, where, and how? *Microorganisms* **6** (3), 75.

604 Gu Z, Pei W, Shen Y, Wang L, Zhu J, *et al.* (2021) Akkermansia muciniphila and its outer protein
605 Amuc_1100 regulates tryptophan metabolism in colitis. *Food Funct.* **12** (20), 10184–10195.

606 Hayase E, Hayase T, Jamal MA, Miyama T, Chang C-C, *et al.* (2022) Mucus-degrading Bacteroides
607 link carbapenems to aggravated graft-versus-host disease. *Cell* **185** (20), 3705–3719.

608 Hepworth MR, Fung TC, Masur SH, Kelsen JR, McConnell FM, *et al.* (2015) Group 3 innate lymphoid
609 cells mediate intestinal selection of commensal bacteria–specific CD4+ T cells. *Science.* **348**
610 (6238), 1031–1035.

611 Horvath TD, Ihekweazu FD, Haidacher SJ, Ruan W, Engevik KA, *et al.* (2022) Bacteroides ovatus

612 colonization influences the abundance of intestinal short chain fatty acids and
613 neurotransmitters. *Iscience* **25** (5), 104158.
614 Hrncir T, Stepankova R, Kozakova H, Hudcovic T, and Tlaskalova-Hogenova H (2008) Gut
615 microbiota and lipopolysaccharide content of the diet influence development of regulatory T
616 cells: studies in germ-free mice. *BMC Immunol.* **9** (1), 1–11.
617 Jangi S, Gandhi R, Cox LM, Li N, von Glehn F, *et al.* (2016) Alterations of the human gut microbiome
618 in multiple sclerosis. *Nat. Commun.* **7** (1), 12015.
619 Kalbermatter C, Fernandez Trigo N, Christensen S, and Ganal-Vonarburg SC (2021) Maternal
620 Microbiota, Early Life Colonization and Breast Milk Drive Immune Development in the Newborn.
621 *Front. Immunol.* **12**, 1768.
622 Kennedy EA, King KY, and Baldridge MT (2018) Mouse microbiota models: comparing germ-free
623 mice and antibiotics treatment as tools for modifying gut bacteria. *Front. Physiol.* **9**, 1534.
624 Kostopoulos I, Elzinga J, Ottman N, Klievink JT, Blijenberg B, *et al.* (2020) Akkermansia muciniphila
625 uses human milk oligosaccharides to thrive in the early life conditions in vitro. *Sci. Rep.* **10** (1),
626 1–17.
627 Li S, Bostick JW, Ye J, Qiu J, Zhang B, *et al.* (2018) Aryl hydrocarbon receptor signaling cell
628 intrinsically inhibits intestinal group 2 innate lymphoid cell function. *Immunity* **49** (5), 915–928.
629 Lin X, Tawch S, Singh A, Morgun A, Shulzhenko N, *et al.* (2021) Akkermansia muciniphila induces
630 Th17 cells by mediating tryptophan metabolism and exacerbates experimental autoimmune
631 encephalomyelitis (EAE). *J. Immunol.* **206** (1 Supplement), 105.09 LP-105.09.
632 Liu Y, Song Y, Lin D, Lei L, Mei Y, *et al.* (2019) NCR− group 3 innate lymphoid cells orchestrate IL-
633 23/IL-17 axis to promote hepatocellular carcinoma development. *EBioMedicine* **41**, 333–344.
634 Liu Y, Yang M, Tang L, Wang F, Huang S, *et al.* (2022) TLR4 regulates RORγt+ regulatory T-cell
635 responses and susceptibility to colon inflammation through interaction with Akkermansia
636 muciniphila. *Microbiome* **10** (1), 1–20.
637 Love MI, Huber W, and Anders S (2014) Moderated estimation of fold change and dispersion for
638 RNA-seq data with DESeq2. *Genome Biol.* **15** (12), 550.

639 Lubin J-B, Green J, Maddux S, Denu L, Duranova T, *et al.* (2023) Arresting microbiome development
640 limits immune system maturation and resistance to infection in mice. *Cell Host Microbe*
641 Luna E, Parkar SG, Kirmiz N, Hartel S, Hearn E, *et al.* (2022) Utilization efficiency of human milk
642 oligosaccharides by human-associated Akkermansia is strain dependent. *Appl. Environ.*
643 *Microbiol.* **88** (1), e01487-21.
644 Macpherson AJ and Harris NL (2004) Interactions between commensal intestinal bacteria and the
645 immune system. *Nat. Rev. Immunol.* **4** (6), 478–485.
646 Martens E, Pereira G, Boudaud M, Wolter M, Alexander C, *et al.* (2023) Unravelling specific diet and
647 gut microbial contributions to inflammatory bowel disease. *ResearchSquare*
648 https://doi.org/10.21203/rs.3.rs-2518251/v1 [PREPRINT]
649 Martin M (2011) Cutadapt removes adapter sequences from high-throughput sequencing reads.
650 *EMBnet. J.* **17** (1), 10–12.
651 Mirpuri J (2021) Evidence for maternal diet-mediated effects on the offspring microbiome and
652 immunity: implications for public health initiatives. *Pediatr. Res.* **89** (2), 301–306.
653 Al Nabhani Z, Dulauroy S, Marques R, Cousu C, Al Bounny S, *et al.* (2019) A Weaning Reaction to
654 Microbiota Is Required for Resistance to Immunopathologies in the Adult. *Immunity* **50** (5),
655 1276–1288.
656 Neumann M, Steimle A, Grant ET, Wolter M, Parrish A, *et al.* (2021) Deprivation of dietary fiber in
657 specific-pathogen-free mice promotes susceptibility to the intestinal mucosal pathogen
658 Citrobacter rodentium. *Gut Microbes*
659 Parrish A, Boudaud M, Grant E, Willieme S, Neumann M, *et al.* (2022) Akkermansia muciniphila
660 regulates food allergy in a diet-dependent manner. *ResearchSquare*
661 https://doi.org/10.21203/rs.3.rs-1745691/v1 [PREPRINT]
662 Parrish A, Grant E, Boudaud M, Hunewald O, Hirayama A, *et al.* (2022) Dietary fibers boost gut
663 microbiota-produced B vitamin pool and alter host immune landscape. *ResearchSquare*
664 https://doi.org/doi.org/10.21203/rs.3.rs-1563674/v2 [PREPRINT]
665 Qiu J, Heller JJ, Guo X, Zong-ming EC, Fish K, *et al.* (2012) The aryl hydrocarbon receptor regulates

666 gut immunity through modulation of innate lymphoid cells. *Immunity* **36** (1), 92–104.
667 Quast C, Pruesse E, Yilmaz P, Gerken J, Schweer T, *et al.* (2013) The SILVA ribosomal RNA gene
668 database project: Improved data processing and web-based tools. *Nucleic Acids Res.*
669 Rey FE, Faith JJ, Bain J, Muehlbauer MJ, Stevens RD, *et al.* (2010) Dissecting the in vivo metabolic
670 potential of two human gut acetogens. *J. Biol. Chem.* **285** (29), 22082–22090.
671 Robertson RC, Manges AR, Finlay BB, and Prendergast AJ (2019) The human microbiome and child
672 growth–first 1000 days and beyond. *Trends Microbiol.* **27** (2), 131–147.
673 Sanos SL, Bui VL, Mortha A, Oberle K, Heners C, *et al.* (2009) RORγt and commensal microflora
674 are required for the differentiation of mucosal interleukin 22–producing NKp46+ cells. *Nat.*
675 *Immunol.* **10** (1), 83–91.
676 Sonnenburg ED, Smits SA, Tikhonov M, Higginbottom SK, Wingreen NS, *et al.* (2016) Diet-induced
677 extinctions in the gut microbiota compound over generations. *Nature* **529** (7585), 212–215.
678 Spidlen J, Breuer K, Rosenberg C, Kotecha N, and Brinkman RR (2012) FlowRepository: A resource
679 of annotated flow cytometry datasets associated with peer-reviewed publications. *Cytom. Part*
680 *A*
681 Steimle A, De Sciscio A, Neumann M, Grant ET, Pereira G V., *et al.* (2021) Constructing a gnotobiotic
682 mouse model with a synthetic human gut microbiome to study host–microbe cross talk. *STAR*
683 *Protoc.* **2** (2)
684 Szanto I, Rubbia-Brandt L, Kiss P, Steger K, Banfi B, *et al.* (2005) Expression of NOX1, a
685 superoxide-generating NADPH oxidase, in colon cancer and inflammatory bowel disease. *J.*
686 *Pathol. A J. Pathol. Soc. Gt. Britain Irel.* **207** (2), 164–176.
687 Takeuchi T, Miyauchi E, Kanaya T, Kato T, Nakanishi Y, *et al.* (2021) Acetate differentially regulates
688 IgA reactivity to commensal bacteria. *Nature* **595** (7868), 560–564.
689 Thorburn AN, McKenzie CI, Shen SJ, Stanley D, Macia L, *et al.* (2015) Evidence that asthma is a
690 developmental origin disease influenced by maternal diet and bacterial metabolites. *Nat.*
691 *Commun.* **6** (1), 7320.
692 Wells JM, Gao Y, de Groot N, Vonk MM, Ulfman L, *et al.* (2022) Babies, Bugs, and Barriers: Dietary

693 Modulation of Intestinal Barrier Function in Early Life. *Annu. Rev. Nutr.* **42**

694 Xie Y-H, Gao Q-Y, Cai G-X, Sun X-M, Zou T-H, *et al.* (2017) Fecal Clostridium symbiosum for
695 noninvasive detection of early and advanced colorectal cancer: test and validation studies.
696 *EBioMedicine* **25**, 32–40.

697 Yoon HS, Cho CH, Yun MS, Jang SJ, You HJ, *et al.* (2021) Akkermansia muciniphila secretes a
698 glucagon-like peptide-1-inducing protein that improves glucose homeostasis and ameliorates
699 metabolic disease in mice. *Nat. Microbiol.* **6** (5), 563–573.

700 Yu G, Wang L-G, Han Y, and He Q-Y (2012) clusterProfiler: an R package for comparing biological
701 themes among gene clusters. *Omi. a J. Integr. Biol.* **16** (5), 284–287.

702 Zheng W, Zhao W, Wu M, Song X, Caro F, *et al.* (2020) Microbiota-targeted maternal antibodies
703 protect neonates from enteric infection. *Nature* **577** (7791), 543–548.

704 Zhu Hai, Wang G, Zhu Haixing, and Xu A (2021) ITGA5 is a prognostic biomarker and correlated
705 with immune infiltration in gastrointestinal tumors. *BMC Cancer* **21** (1), 1–14.

706 ## Figure legends

707 **Figure 1. Delayed expansion of *Akkermansia* among offspring of fiber-deprived dams.**

708 A. Schematic representation of the study design.

709 B. Stream plot showing the relative abundance of the 14 bacterial strains in the colons of pups born
710 to 14SM FF-fed mice, 14SM FR-fed mice and 13SM FR-fed dams. Abundances represent an
711 average of all pups at the specified age. Distal colon contents were analyzed by qPCR using
712 primers against targets that are unique to each bacteria and present once per genome. Asterisk
713 indicates bacterial strains that were considered absent (average abundance <0.1%) in the pups.

714 C. Line plots of the mean relative abundances and SD of each bacterial strain from ages 10 to 30
715 days. For non-AM strains, relative abundances of the 14SM groups were recalculated excluding
716 AM in order to compare abundances with the 13SM group.

717 Data information: Strain abundances were normally distributed within each group according to the
718 Kolmogorov-Smirnov test. Statistical significance compared to the 14SM FR control at each time
719 point was calculated by two-way ANOVA with false-discovery adjustment using the Benjamini and
720 Hochberg method. Adjusted *p* values are indicated for 14SM FF vs 14SM FR (red) and 13SM FR vs
721 14SM FR (orange). Data are from two independent experiments and represent biological replicates
722 (n = 2–11/group).

723

724 **Figure 2. Maternal diet alters colonic transcriptome of offspring at age 15 days.**

725 A. Table depicting counts of genes with differential transcription across groups after filtering reads
726 not present at least once across all samples (top; see **Dataset EV5, Dataset EV6**) and
727 differentially enriched gene sets between groups according to the Gene Ontologies (GO) terms
728 for biological processes (bottom; see **Dataset EV7**).

729 B. Volcano plot showing gene abbreviations for colonic transcripts that were significantly enriched
730 in 14SM FF or 14SM FR after correction for multiple comparisons using DESeq2 (see **Dataset**
731 **EV5**).

732 C. Category netplots displaying gene sets for biological processes and their associated genes that
733 were differentially represented in pups born to 14SM FF vs 14SM FR dams. Top five up- and
734 down-regulated gene sets for biological processes are shown; all gene sets can be found in
735 **Dataset EV7**.
736 D. mRNA expression of *Ifng*, *Tnfa*, *Il17f*, and *Il22*. Colonic transcription levels were normalized by
737 *Hprt*, which was the most stable among the three housekeeping genes tested (*Hprt, Hsp90,*
738 *Gapdh)*. Longitudinal data of mean ± SEM is shown for 14SM FF, 14SM FR, and 13SM FR pups
739 at age 10-20 days (circles) with statistical significance calculated using two-way ANOVA factored
740 on group and time point compared to the 14SM FR control. To the right of each longitudinal plot,
741 we also report colonic transcript levels for pups born to germ-free (GF) FF or FR dams at age 15
742 days (squares) with statistical significance based on a one-way ANOVA with false-discovery
743 adjustment using the Benjamini and Hochberg method. Outliers removed using ROUT method
744 with Q = 10%. Data are from two independent experiments and represent biological replicates
745 (n = 3–20/group).
746
747 **Figure 3. Maternal diet and microbiome shape innate and adaptive neonatal immune cell**
748 **populations.**
749 A. For mice at age 15 days, the proportion of cytotoxic natural killer (cNK), innate lymphoid cell
750 (ILC) type 1, ILC type 2, ILC type 3, natural cytotoxicity receptor (NCR) positive ILC3, and NCR
751 negative ILC3 populations among $CD45^+$ cells.
752 B. For mice at age 15 days, the proportion of $CD8^+$ T cells, $CD4^+$ T cells, Tregs (total $FoxP3^+$), Th1
753 cells ($T\text{-}bet^+FoxP3^-$), Th2 ($GATA3^+FoxP3^-$), and Th17 ($RORgt^+FoxP3^-$) populations among
754 $CD45^+$ cells.
755 Statistical significance is based on a one-way ANOVA with false-discovery adjustment using the
756 Benjamini and Hochberg method. Data are from two independent experiments and represent
757 biological replicates (n = 8–20/group).
758

759 **Figure 4. Summary of key transcriptional, cellular, and microbial shifts among pups of 14SM**
760 **fiber-deprived dams.** Maternal milk components (immunoglobulins, altered milk glycan structures)
761 among fiber-deprived dams are predicted to inhibit the establishment of mucin-degrading bacteria in
762 the suckling period, after which this functional group rapidly expands, following a pattern inverse to
763 pups of FR-fed dams. These microbial changes are accompanied by an array of host changes
764 characterized by colonic transcripts involved in epithelial development and innate defense signaling
765 as well as differential development of key immune cell subsets.
766
767 **Table 1.** Primers for RT-qPCR against colonic cDNA transcript library.
768

769 ## Expanded View

770 **Figure EV1.**

771 A. PCA plot of the top 500 most variable genes among samples analyzed by RNA sequencing (*n* =
772 4 mice/group).
773 B. Volcano plot showing colonic transcripts that were significantly enriched in 14SM FR or 13SM
774 FR after correction for multiple comparisons using DESeq2 (*n* = 3-4 mice/group).
775 C. mRNA expression of *Il12p40* and *Il23*, targeted transcripts of interest (*n* = 17-24 mice/group).
776 D. mRNA expression of *Ifit1b1*, transcript identified by RNA sequencing as elevated in 13SM FR.
777 E. mRNA expression of transcripts belonging to top 5 GO gene sets elevated in 14SM FR (*Nlrbp1*
778 and *Ppp3r2*) or 14SM FF (*Igtp*, *Tgtp2*, *Gbp2*, *Nox1*, *Hspb2*, *Fos*, *Clca3a2*, *Itga5*, *a*nd *F13a1*).
779 Colonic transcription levels were normalized by *Hprt*, which was the most stable among the three
780 housekeeping genes tested (*Hprt, Hsp90, Gapdh)*.

781 Data information: Longitudinal data of mean ± SEM is shown for 14SM FF, 14SM FR, and 13SM FR
782 pups at age 10-20 days (circles) with statistical significance calculated using two-way ANOVA
783 factored on group and time point compared to the 14SM FR control. To the right of each longitudinal
784 plot, we also report colonic transcript levels for pups born to germ-free (GF) FF or FR dams at age
785 15 days (squares) with statistical significance based on a one-way ANOVA with false-discovery

786 adjustment using the Benjamini and Hochberg method. Outliers removed using ROUT method with
787 Q = 10%.
788
789 **Figure EV2.** Representative gating strategy for flow cytometry analysis.
790
791 **Figure EV3.**
792 A. Number of pups born per litter in each group. (*n* = 2-3 litters/group). No statistical significance
793 for pairwise comparisons based on a one-way ANOVA with false-discovery adjustment using
794 the Benjamini and Hochberg method.
795 B. Pup weights at the specified intervals. (*n* = 2-17 mice/group). Longitudinal data of mean
796 weight (g) ± SEM is shown for 14SM FF, 14SM FR, and 13SM FR pups at age 10-30 days
797 (circles) with statistical significance calculated using two-way ANOVA factored on group and
798 time point compared to the 14SM FR control. To the right, we also report weights of pups
799 born to germ-free (GF) FF or FR dams at age 15 days (squares) with statistical significance
800 based on a one-way ANOVA with false-discovery adjustment using the Benjamini and
801 Hochberg method.
802
803 **Figure EV4.** Correlation coefficient (R^2) for the linear trendline fit to relative abundance by qPCR (y-
804 axis) versus relative abundance by 16S rRNA gene sequencing (x-axis). Plots shown for all bacteria
805 that were present at a detectable level in the pups of dams colonized with 13SM or 14SM.
806
807 **Dataset EV1.** Abundances of synthetic microbiota (SM) members among parent mice by qPCR.
808 Compositions are based on fecal samples taken at the end of the study.
809
810 **Dataset EV2.** Abundances of synthetic microbiota (SM) members among individual pups by qPCR.
811
812 **Dataset EV3.** 16S rRNA gene sequencing to rule out contamination with non-14SM bacteria.

813

814 **Dataset EV4.** Count table of colonic transcripts mapping to genes by ENSEMBL identifier. Asterisk
815 (*) indicates samples identified as outliers by PCA plotting (**Fig EV1A**).

816

817 **Dataset EV5.** Differential enrichment analysis using DESeq2 for 14SM fiber-free and 14SM fiber-
818 rich contrasts.

819

820 **Dataset EV6.** Differential enrichment analysis using DESeq2 for 14SM fiber-rich and 13SM fiber-
821 rich contrasts.

822

823 **Dataset EV7.** Gene set differential enrichment analysis using clusterProfiler (biological processes)
824 for 14SM fiber-free and 14SM fiber-rich contrasts.

825

826 **Dataset EV8.** RefFinder results to identify most stable housekeeping gene.

Fig1

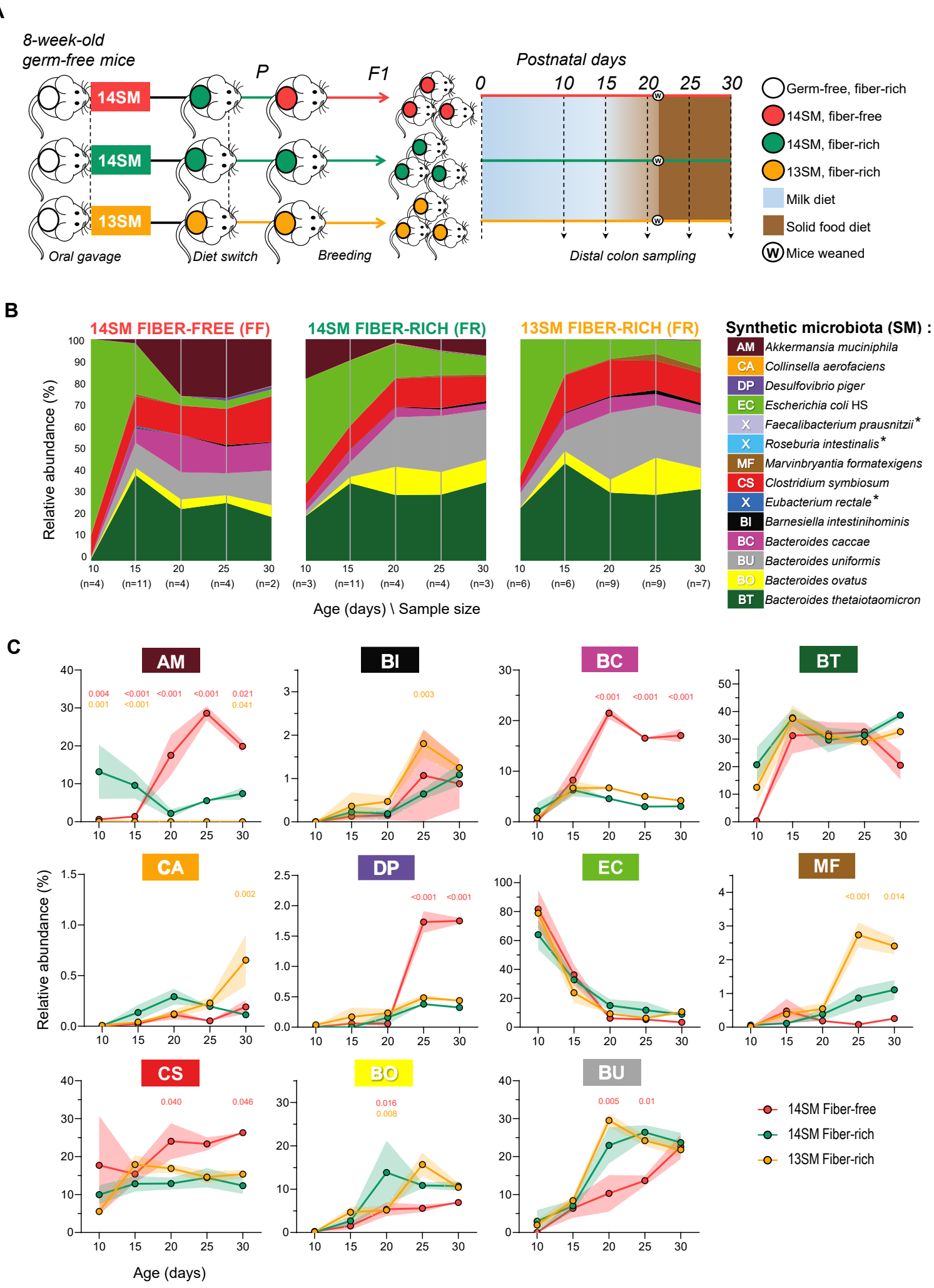
A
8-week-old germ-free mice
14SM
14SM
13SM
P
F1
Postnatal days
0
10
15
20
25
30
Oral gavage
Diet switch
Breeding
Distal colon sampling
Germ-free, fiber-rich
14SM, fiber-free
14SM, fiber-rich
13SM, fiber-rich
Milk diet
Solid food diet
Mice weaned
B
14SM FIBER-FREE (FF)
14SM FIBER-RICH (FR)
13SM FIBER-RICH (FR)
Relative abundance (%)
Age (days) \ Sample size
Synthetic microbiota (SM) :
AM Akkermansia muciniphila
CA Collinsella aerofaciens
DP Desulfovibrio piger
EC Escherichia coli HS
X Faecalibacterium prausnitzii*
X Roseburia intestinalis*
MF Marvinbryantia formatexigens
CS Clostridium symbiosum
X Eubacterium rectale*
BI Barnesiella intestinihominis
BC Bacteroides caccae
BU Bacteroides uniformis
BO Bacteroides ovatus
BT Bacteroides thetaiotaomicron
C
AM
BI
BC
BT
CA
DP
EC
MF
CS
BO
BU
Relative abundance (%)
Age (days)
14SM Fiber-free
14SM Fiber-rich
13SM Fiber-rich

Fig2

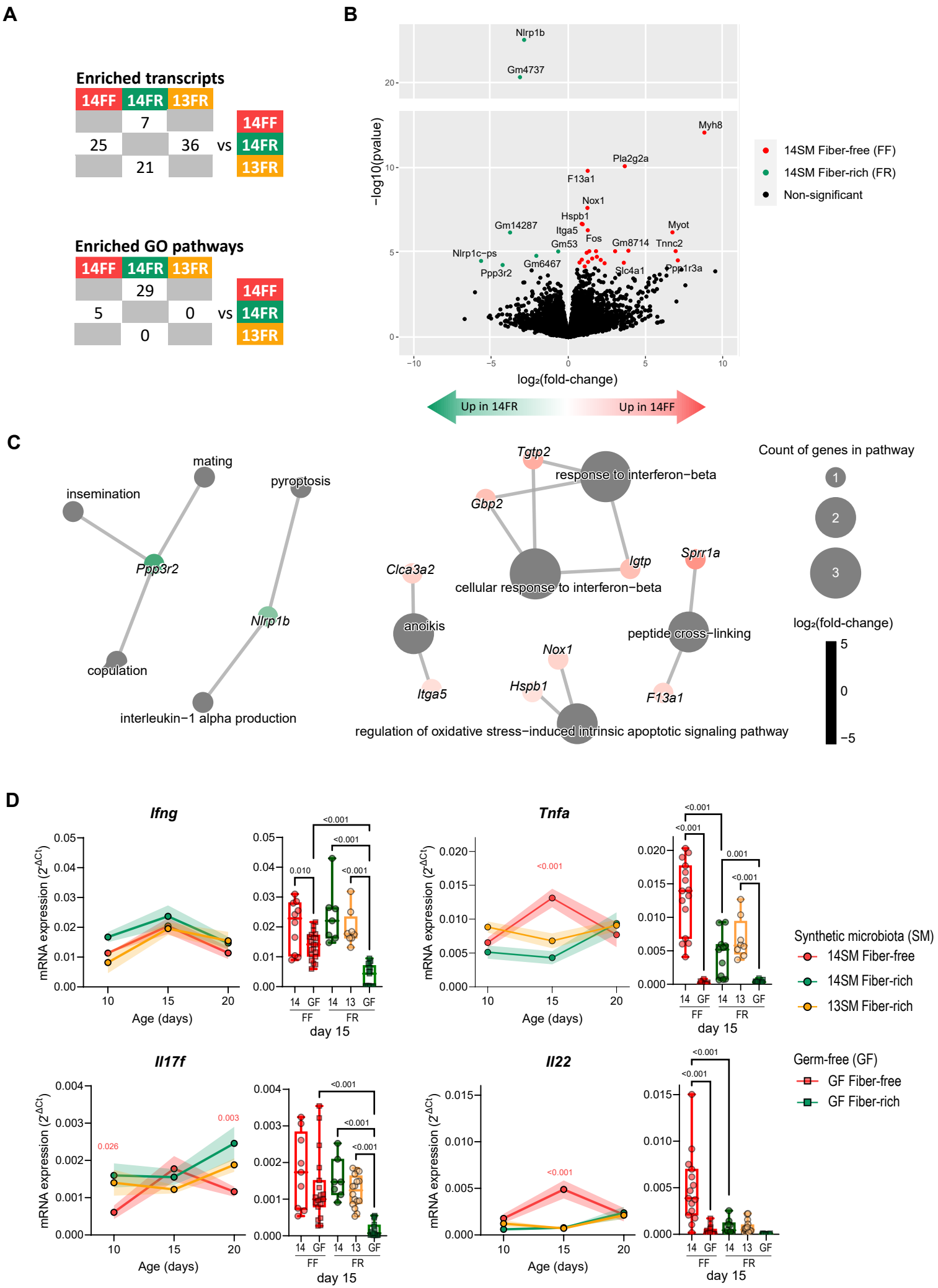
A
Enriched transcripts
14FF 14FR 13FR
7
25 36 vs 14FF 14FR 13FR
21
Enriched GO pathways
14FF 14FR 13FR
29
5 0 vs 14FF 14FR 13FR
0
B
Nlrp1b
Gm4737
Myh8
Pla2g2a
F13a1
Nox1
Hspb1
Itga5
Fos
Gm53
Gm8714
Tnnc2
Myot
Gm14287
Nlrp1c−ps
Ppp3r2
Gm6467
Slc4a1
Ppp1r3a
−log10(pvalue)
log2(fold-change)
14SM Fiber-free (FF)
14SM Fiber-rich (FR)
Non-significant
Up in 14FR
Up in 14FF
C
mating
insemination
pyroptosis
Ppp3r2
Nlrp1b
copulation
interleukin−1 alpha production
Tgtp2
response to interferon−beta
Gbp2
Igtp
Sprr1a
Clca3a2
cellular response to interferon−beta
anoikis
peptide cross−linking
Nox1
Hspb1
Itga5
F13a1
regulation of oxidative stress−induced intrinsic apoptotic signaling pathway
Count of genes in pathway
1
2
3
log2(fold-change)
5
0
−5
D
Ifng
Tnfa
Il17f
Il22
mRNA expression (2^ΔCt)
Age (days)
day 15
FF
FR
Synthetic microbiota (SM)
14SM Fiber-free
14SM Fiber-rich
13SM Fiber-rich
Germ-free (GF)
GF Fiber-free
GF Fiber-rich

Fig3

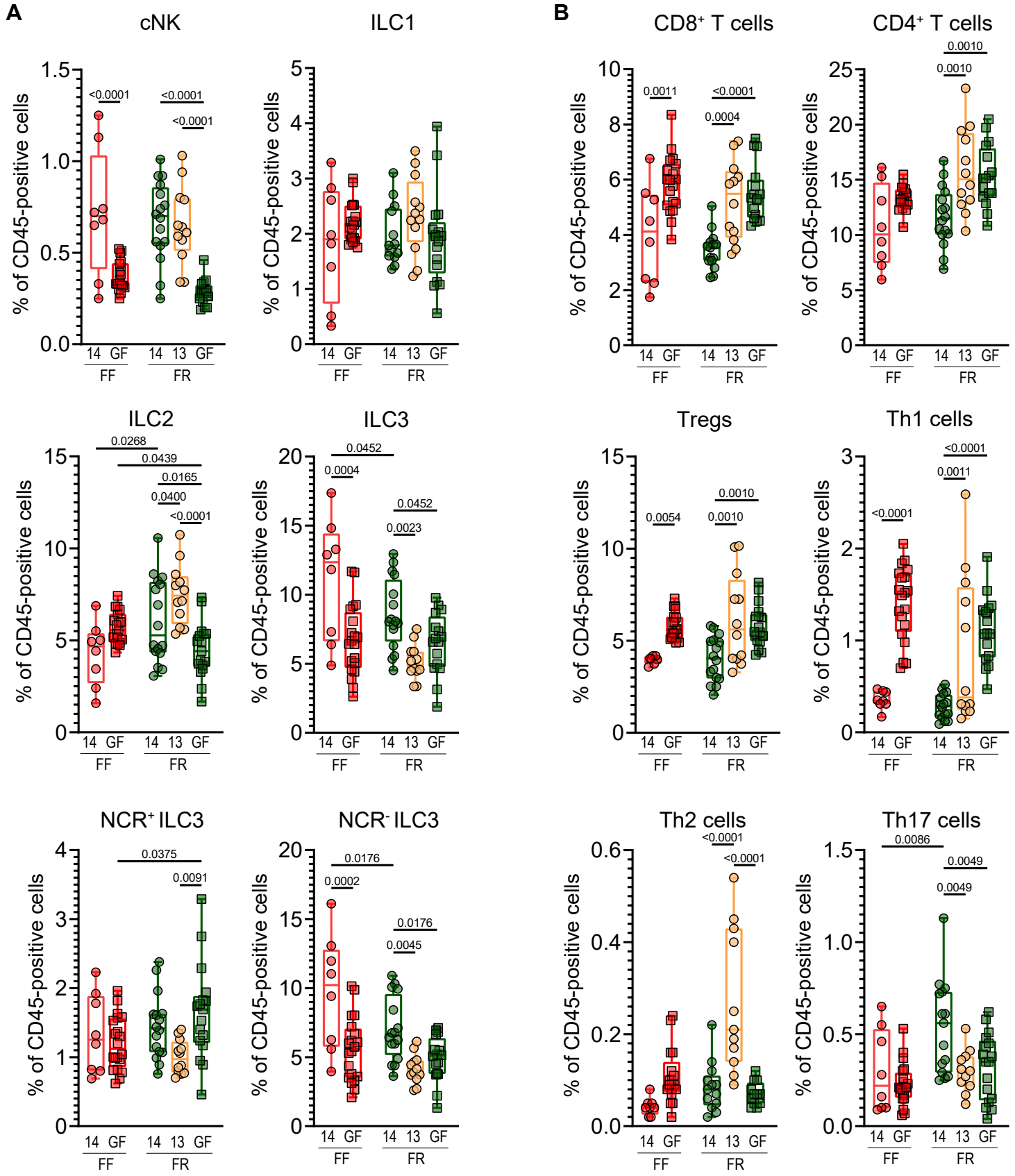
A
cNK
ILC1
ILC2
ILC3
NCR⁺ ILC3
NCR⁻ ILC3
B
CD8⁺ T cells
CD4⁺ T cells
Tregs
Th1 cells
Th2 cells
Th17 cells
% of CD45-positive cells
14 GF 14 13 GF
FF FR
<0.0001
0.0268
0.0439
0.0165
0.0400
0.0452
0.0004
0.0023
0.0375
0.0091
0.0176
0.0002
0.0045
0.0011
0.0054
0.0010
0.0086
0.0049

Fig4

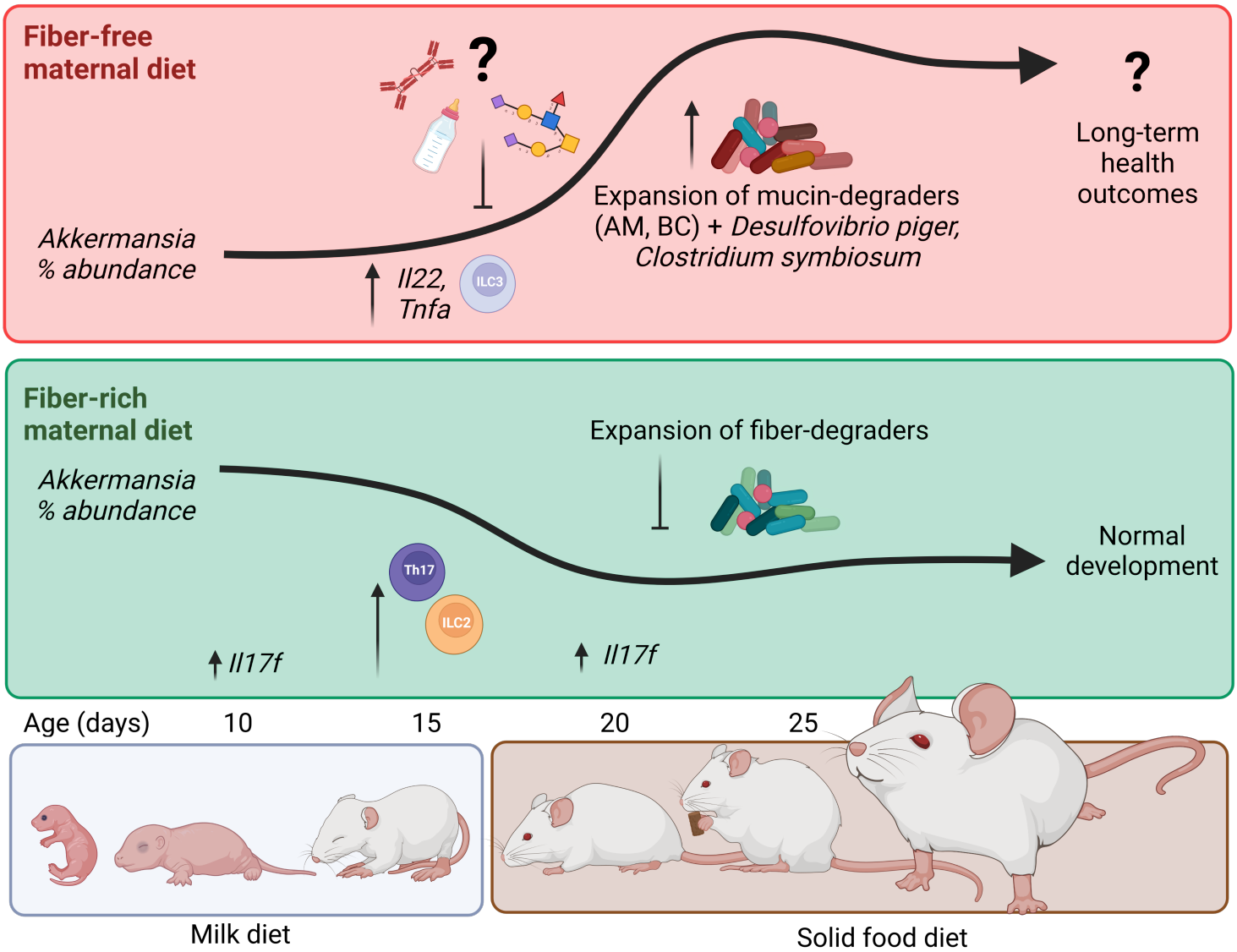
Fiber-free maternal diet
?
Akkermansia % abundance
Il22, Tnfa
ILC3
Expansion of mucin-degraders (AM, BC) + Desulfovibrio piger, Clostridium symbiosum
?
Long-term health outcomes
Fiber-rich maternal diet
Akkermansia % abundance
Expansion of fiber-degraders
Th17
ILC2
Il17f
Il17f
Normal development
Age (days)
10
15
20
25
Milk diet
Solid food diet

FigEV1

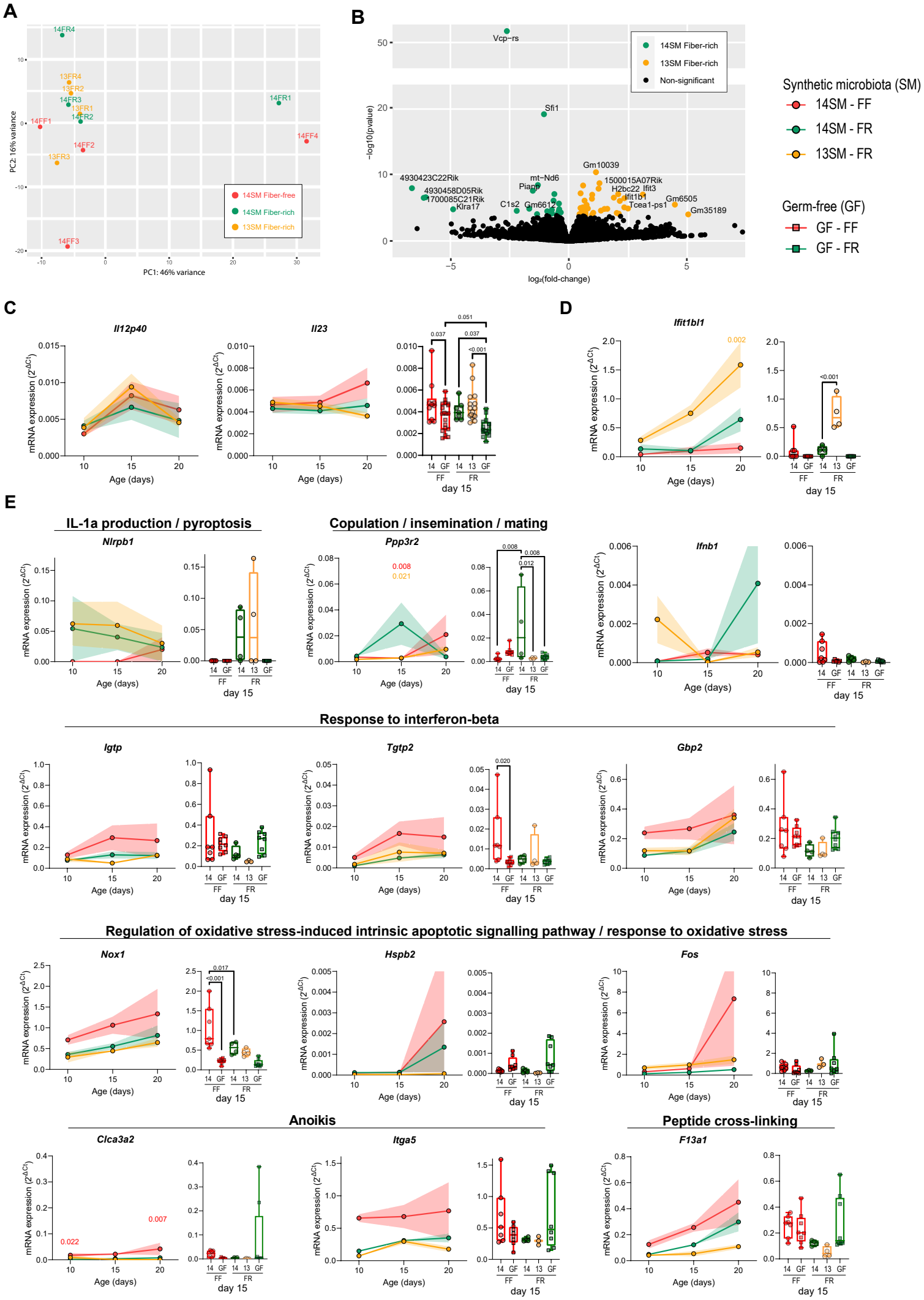
A
PC2: 16% variance
PC1: 46% variance
14SM Fiber-free
14SM Fiber-rich
13SM Fiber-rich
B
−log10(pvalue)
log2(fold-change)
Vcp−rs
Sfi1
Gm10039
4930423C22Rik
mt−Nd6
Pian6
1500015A07Rik
H2bc22
Ifit3
Ifit1bl1
Tcea1-ps1
Gm6505
Gm35189
4930458D05Rik
1700085C21Rik
Klra17
C1s2
Gm6612
14SM Fiber-rich
13SM Fiber-rich
Non-significant
Synthetic microbiota (SM)
14SM - FF
14SM - FR
13SM - FR
Germ-free (GF)
GF - FF
GF - FR
C
Il12p40
Il23
mRNA expression (2^ΔCt)
Age (days)
day 15
D
Ifit1bl1
E
IL-1a production / pyroptosis
Nlrpb1
Copulation / insemination / mating
Ppp3r2
Ifnb1
Response to interferon-beta
Igtp
Tgtp2
Gbp2
Regulation of oxidative stress-induced intrinsic apoptotic signalling pathway / response to oxidative stress
Nox1
Hspb2
Fos
Anoikis
Clca3a2
Itga5
Peptide cross-linking
F13a1

FigEV2

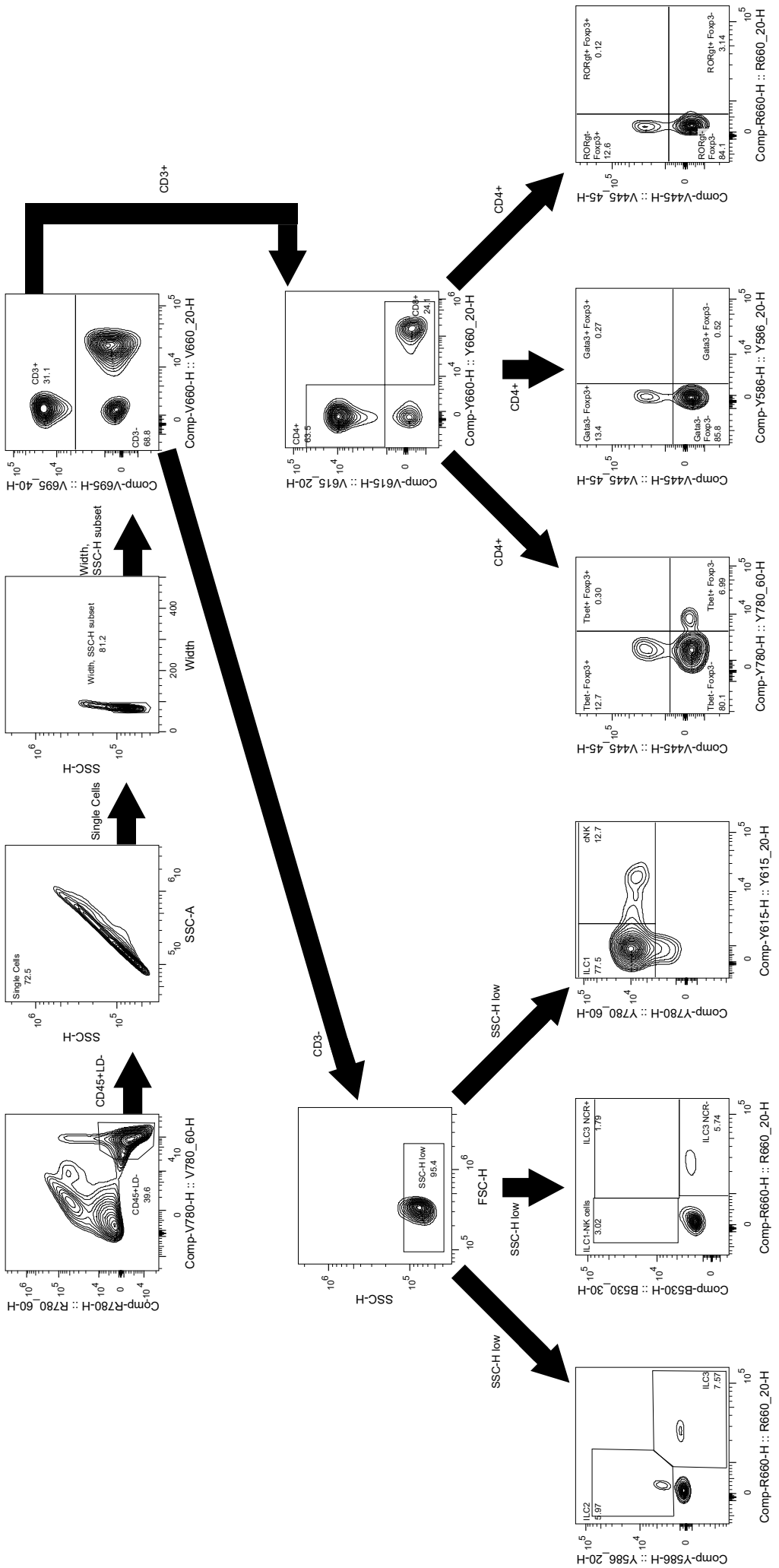
Comp-R780-H :: R780_60-H
Comp-V780-H :: V780_60-H
CD45+LD-
CD45+LD-
39.6
SSC-H
Single Cells
Single Cells
72.5
SSC-A
SSC-H
Width, SSC-H subset
Width, SSC-H subset
81.2
Width
Comp-V695-H :: V695_40-H
Comp-V660-H :: V660_20-H
CD3+
CD3+
31.1
CD3-
68.8
CD3+
CD3-
SSC-H
SSC-H low
95.4
FSC-H
Comp-V615-H :: V615_20-H
Comp-Y660-H :: Y660_20-H
CD4+
CD4+
63.5
CD3+
24.1
CD4+
CD4+
CD4+
Comp-V445-H :: V445_45-H
Comp-Y780-H :: Y780_60-H
Tbet- Foxp3+
12.7
Tbet+ Foxp3+
0.30
Tbet- Foxp3-
80.1
Tbet+ Foxp3-
6.99
Comp-V445-H :: V445_45-H
Comp-Y586-H :: Y586_20-H
Gata3- Foxp3+
13.4
Gata3+ Foxp3+
0.27
Gata3- Foxp3-
85.8
Gata3+ Foxp3-
0.52
Comp-V445-H :: V445_45-H
Comp-R660-H :: R660_20-H
RORgt- Foxp3+
12.6
RORgt+ Foxp3+
0.12
RORgt- Foxp3-
84.1
RORgt+ Foxp3-
3.14
SSC-H low
SSC-H low
SSC-H low
Comp-Y780-H :: Y780_60-H
Comp-Y615-H :: Y615_20-H
ILC1
77.5
cNK
12.7
Comp-B530-H :: B530_30-H
Comp-R660-H :: R660_20-H
ILC1-NK cells
3.02
ILC3 NCR+
1.79
ILC3 NCR-
5.74
Comp-Y586-H :: Y586_20-H
Comp-R660-H :: R660_20-H
ILC2
4.97
ILC3
7.57

FigEV3

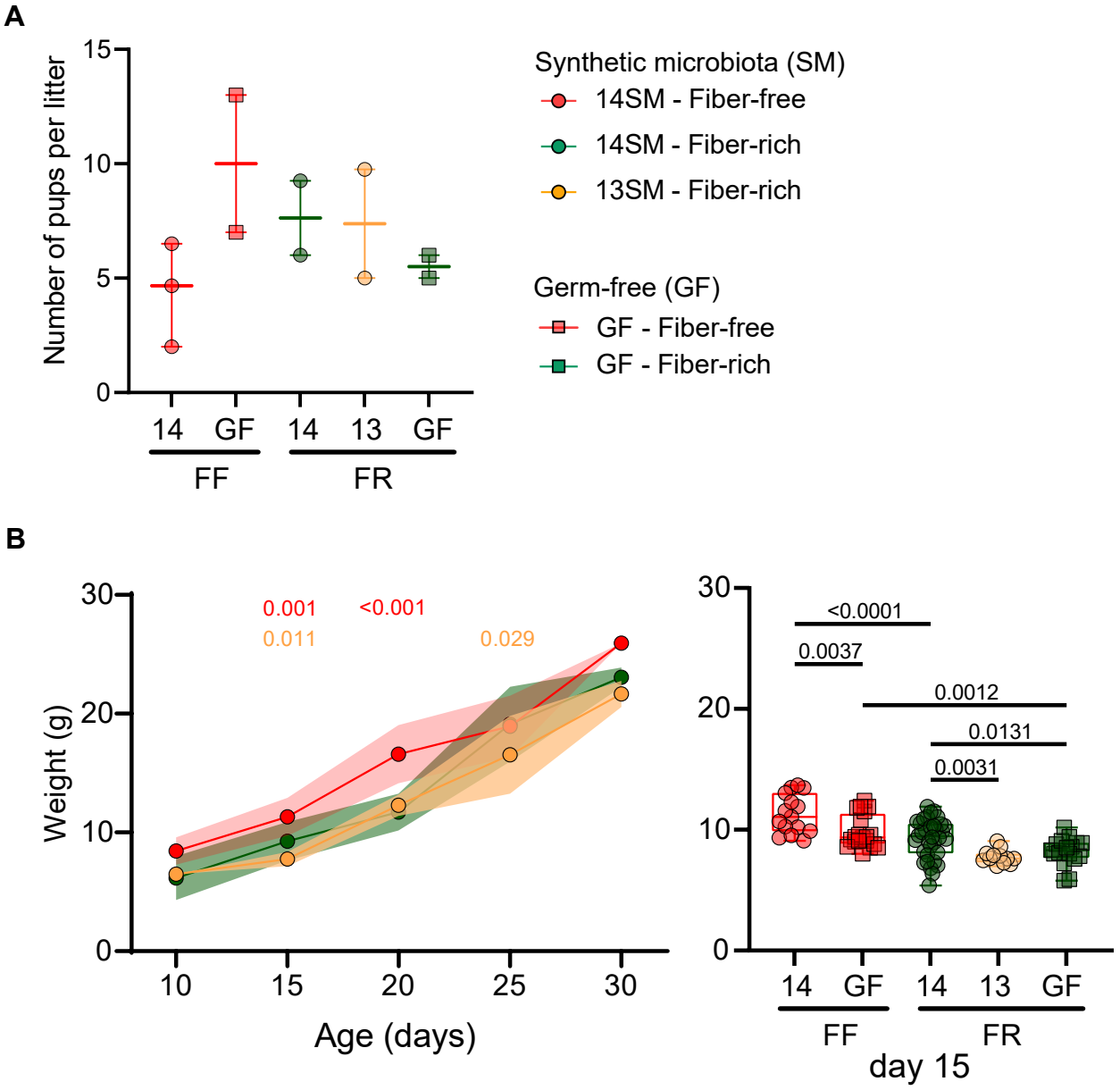
A
Number of pups per litter
15
10
5
0
14
GF
14
13
GF
FF
FR
Synthetic microbiota (SM)
14SM - Fiber-free
14SM - Fiber-rich
13SM - Fiber-rich
Germ-free (GF)
GF - Fiber-free
GF - Fiber-rich
B
Weight (g)
30
20
10
0
0.001
<0.001
0.011
0.029
10
15
20
25
30
Age (days)
<0.0001
0.0037
0.0012
0.0131
0.0031
day 15

FigEV4

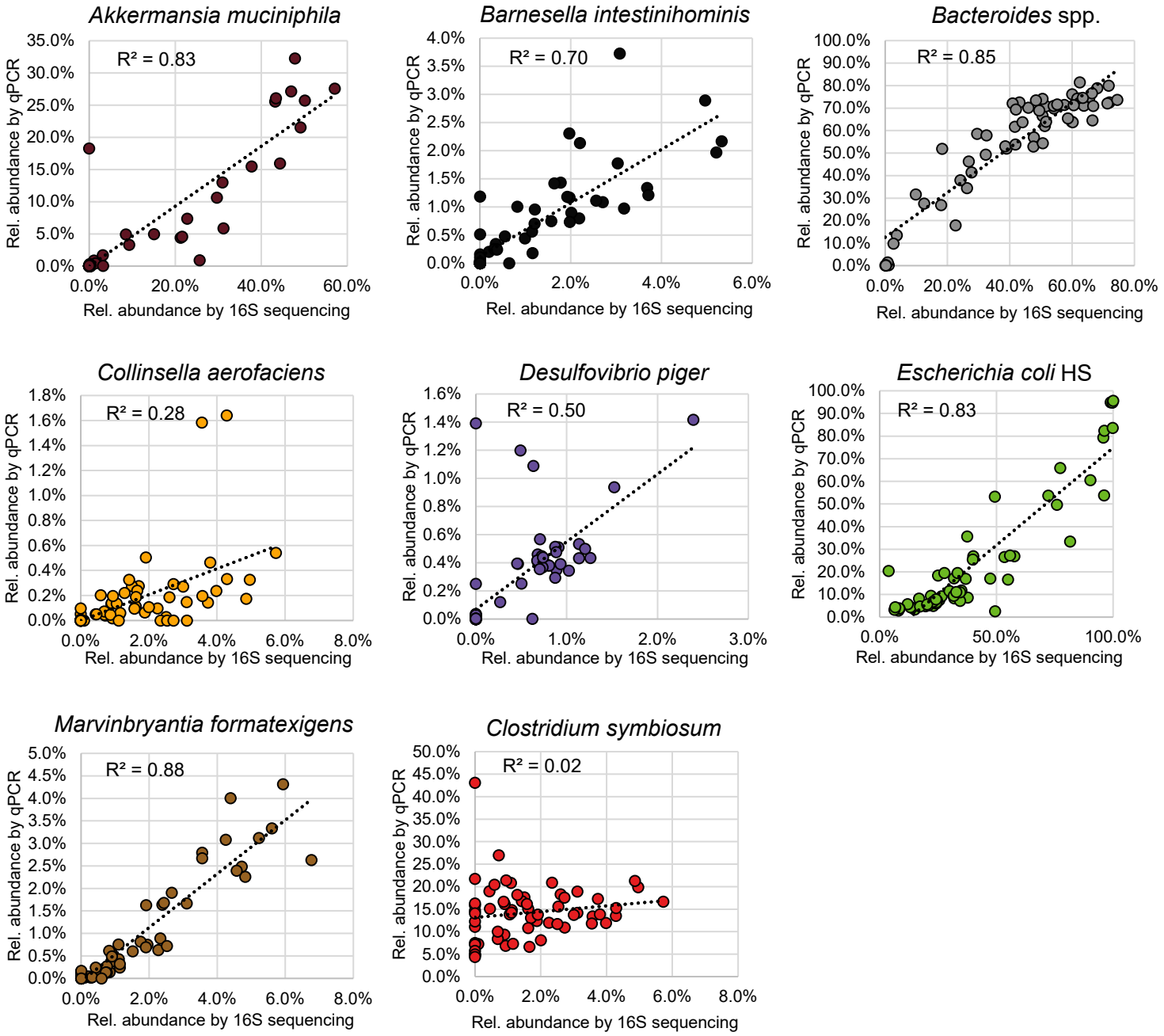
Akkermansia muciniphila
R² = 0.83
Barnesella intestinihominis
R² = 0.70
Bacteroides spp.
R² = 0.85
Collinsella aerofaciens
R² = 0.28
Desulfovibrio piger
R² = 0.50
Escherichia coli HS
R² = 0.83
Marvinbryantia formatexigens
R² = 0.88
Clostridium symbiosum
R² = 0.02
Rel. abundance by qPCR
Rel. abundance by 16S sequencing